LIBRARY
Michigan State
University

This is to certify that the

dissertation entitled

Two-photon Spectroscopy of Quadruply Bonded Metal Dimers:

An Investigation of Zwitterionic Excited States

presented by

Daniel Scott Engebretson

has been accepted towards fulfillment
of the requirements for

MS degree in Chemistry

Daniel G. Nocera George Leroi
Major professor

Date 16 May 1998

MSU is an Affirmative Action/Equal Opportunity Institution

O-12771

PLACE IN RETURN BOX to remove this checkout from your record.
TO AVOID FINES return on or before date due.
MAY BE RECALLED with earlier due date if requested.

DATE DUE	DATE DUE	DATE DUE

6/01 c:/CIRC/DateDue.p65-p.15

TWO-PHOTON SPECTROSCOPY OF QUADRUPLY BONDED METAL DIMERS: AN INVESTIGATION OF ZWITTERIONIC EXCITED STATES

By

Daniel Scott Engebretson

A Thesis

Submitted to
Michigan State University
in partial fulfillment of the requirements
for the degree of

MASTER OF SCIENCE

Department of Chemistry

1998

ABSTRACT

TWO-PHOTON SPECTROSCOPY OF QUADRUPLY BONDED METAL DIMERS: AN INVESTIGATION OF ZWITTERIONIC EXCITED STATES

By

Daniel Scott Engebretson

Two electrons in two weakly coupled orbitals give rise to two states (diradical) with electrons residing in separate orbitals and two states (zwitterionic) with both electrons paired in one orbital or the other. This two-center, two-electron state manifold has eluded experimental confirmation because the zwitterionic states have been difficult to locate. Two-photon excitation of fluorescence of quadruply bonded metal dimers has been utilized to reveal the zwitterionic nature of the singlet excited states of the δ-manifold. The assignment of the band observed in the two-photon fluorescence excitation spectra to the hidden zwitterionic state (2^1A_{1g}) has been aided by measuring the quadratic dependence of the fluorescence on the incident laser intensity and measuring the relative intensity when two circularly polarized photons are used as compared to two linearly polarized photons.

TABLE OF CONTENTS

LIST OF TABLES

LIST OF FIGURES

Chapter I

Introduction

The δ bond has been an enigma since its discovery in 1964 with the preparation and characterization of the octachlorodirhenate ion, $Re_2Cl_8^{2-}$.[1] The electronic configuration was proposed by Cotton to be $\sigma^2\pi^4\delta^2$, implying a sigma bond, two pi bonds and a delta bond between the two rhenium atoms. This configuration explained the observed diamagnetism and the short metal-metal bond distance, as well as the eclipsed geometry of the Cl^- ligands that was determined in the crystal structure of $K_2Re_2Cl_8 \cdot H_2O$. Although the existence of the δ bond was questioned years thereafter, the spectroscopy and calculations of the 70s and 80s confirmed its existence.

The spectroscopic work was pioneered by Cowman and Gray's polarized electronic absorption spectroscopy of single crystal $Re_2Cl_8^{2-}$.[2] This study revealed the lowest energy transition to be polarized along the Re—Re internuclear axis (z-polarized), and a progression with a spacing of 248 cm^{-1} was consistent with the ground state metal-metal stretching frequency of 274 cm^{-1} reported in early Raman work.[3] These observations led to an assignment of the absorption as the $\delta^2 \rightarrow {}^1\delta\delta^*$ (${}^1(\delta \rightarrow \delta^*)$) transition. Early

calculations performed on quadruply bonded dimers were tenuous at best. Calculations carried out by Benard indicated that the $Re_2Cl_8^{2-}$ anion should possess a staggered D_{4d} geometry and that this conformation would be 60 kcal/mole more stable than the experimentally observed eclipsed D_{4h} structure.[4] Furthermore, these calculations indicated that the ground state of the molecule would be a paramagnetic triplet state, in contrast to the observed diamagnetism. As computers became more powerful, it became possible to expand the basis set for the calculations to include multiconfigurational interactions. Taking advantage of this, Hay was able to perform calculations on $Re_2Cl_8^{2-}$ that qualitatively agreed with experimental observations.[5] While these calculations differed from experiment in some respects, such as the $^1(\delta \rightarrow \delta^*)$ excitation energy (calculated = 23,000 - 30,500 cm^{-1}; observed = 14,500 cm^{-1}), they did result in the proper geometry (D_{4h}) and electronic configuration $\sigma^2\pi^4\delta^2$.

I.A. Electronic Structure of Quadruply Bonded Metal-Metal Complexes

The δ bond, a feature unique to quadruply bonded metal-metal (M—M) dimers, is formed by the overlap of two atomic d_{xy} orbitals on adjacent metals as shown in the molecular orbital diagram (Figure I.1). Even though the metal centers are very close to one another (~2.2 Å),[6] there is very little overlap of the parent d_{xy} orbitals owing to their parallel disposition.[7] This leads to a very weak bond, as was encountered early in the study of these systems.

The weakness of the δ bond was first recognized in the spectroscopy of $Re_2Cl_8^{2-}$.[7] While the $^1A_{2u} \leftarrow {}^1A_{1g}$ $^1(\delta \rightarrow \delta^*)$ transition is dipole and spin allowed, it is quite weak (ε_{max} = 1530 $M^{-1}cm^{-1}$). Generally, one electron charge transfer transitions such as this give rise to very intense absorptions ($\varepsilon_{max} \cong 15000$ $M^{-1}cm^{-1}$).[8] It has been shown by Mulliken, however, that charge transfer transitions become less intense as the coupling between the parent atomic orbitals becomes weak.[8] The parameter that governs the

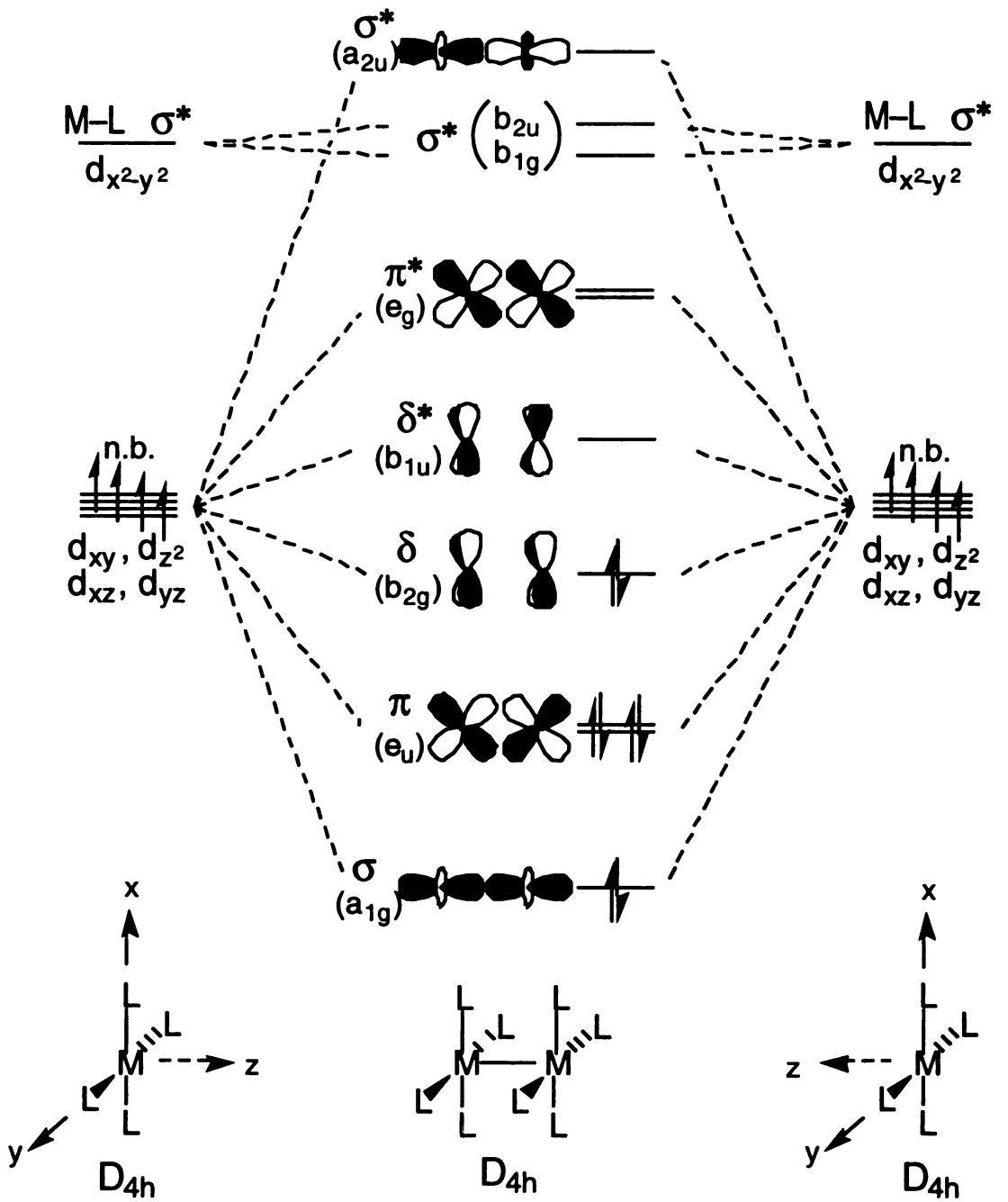

Figure I.1. The Molecular Orbital Diagram for the formation of M_2L_8 from two ML_4 fragments.

intensity of a transition is the oscillator strength, *f*, which is related to the orbital overlap (and hence the bond strength):

$$f = 1.096 \times 10^{11}\, \bar{\nu} S^2 r^2 \qquad \text{(I.1)}$$

where $\bar{\nu}$ is the transition energy (cm^{-1}), S is the overlap of the parent atomic orbitals, and r is the internuclear separation. For the $^1(\delta \rightarrow \delta^*)$ transition for $Re_2Cl_8^{2-}$, $f = 0.023$. When the internuclear separation, determined by X-ray crystallography, is substituted into Equation I.1, S is determined to be ~ 0.1.[7]

The weakness of the δ bond is further supported by the spectroscopy of the one electron oxidized or reduced congeners of quadruply bonded molecules. In these molecules, the ground state electronic configuration is $\sigma^2\pi^4\delta^1$ or $\sigma^2\pi^4\delta^2\delta^*$, which leads to a formal bond order of 3.5. Despite the difference in ground state electronic configuration, however, the structural parameters, including the internuclear separation and hence the orbital overlap, remain quite constant, with typical bond length changes on the order of 0.05Å for each δ electron removed or added.[9] In the oxidized species, where there is only a single electron in the δ orbital, there are no two-electron energies such as electron correlation energy. Because of this, the one electron $^2(\delta \rightarrow \delta^*)$ transition between the δ and δ* molecular orbitals provides a direct measure of the δ bond strength.[10] The situation is similar for the reduced species.[10] The $^2(\delta \rightarrow \delta^*)$ transition for a number of these oxidized and reduced molecules have been measured; they are collected, along with the $^1(\delta \rightarrow \delta^*)$ transitions of their quadruply bonded counterparts and bond length change, in Table I.1. It can be seen that most of the $^2(\delta \rightarrow \delta^*)$ transitions occur between 1400 nm and 1600 nm (7,000 cm^{-1} and 6,000 cm^{-1}). This indicates that the δ bond is very weak when compared to typical sigma and pi bonds (15,000 cm^{-1} to 30,000 cm^{-1}).[11] A few of the tabulated molecules have a $^2(\delta \rightarrow \delta^*)$ transition somewhat higher in energy, but the $^1(\delta \rightarrow \delta^*)$ transition energy of their quadruply bonded counterparts is also higher in energy.

Table I.1. Comparison of the $^1(\delta \rightarrow \delta^*)$ excitation energy and $^2(\delta \rightarrow \delta^*)$ excitation energy and bond length changes for some selected quadruply bonded dimers and their one-electron oxidized counterparts. Values were obtained from reference 10, except for the $Mo_2[O_2P(OC_6H_5)_2]_4^{+/0}$ pair which was obtained from Chang, I. J.; Nocera, D. G., *Inorg. Chem.*, **1989**, *28*, 4309.

Compound	$^2(\delta \rightarrow \delta^*)$ (cm^{-1})	Compound	$^1(\delta \rightarrow \delta^*)$ (cm^{-1})	Bond Length Change
$Mo_2(O_2CPr^n)_4^+$	13300	$Mo_2(O_2CPr^n)_4$	22700	--
$Mo_2(SO_4)_4^{3-}$	7140	$Mo_2(SO_4)_4^{4-}$	19420	0.05Å
$W_2Cl_4(PMe_3)_4^+$	7350	$W_2Cl_4(PMe_3)_4$	15150	--
$Mo_2[O_2P(OC_6H_5)_2]_4^+$	6800	$Mo_2[O_2P(OC_6H_5)_2]_4$	19400	0.04 Å
$Mo_2(HPO_4)_4^{3-}$	6950	$Mo_2(HPO_4)_4^{4-}$	19400	--

-- unknown value

Electrons that reside in weakly coupled orbitals have been a point of theoretical interest for several decades. The two classic examples are the stretched hydrogen molecule and the twisted ethylene molecule. The case of stretched hydrogen was first investigated by Mulliken in his explanation of the electronic spectra of homonuclear diatomic molecules.[12] Later, the stretched hydrogen molecule gained considerable attention when it was investigated by Coulson and Fischer.[13] At dihydrogen's equilibrium geometry there is very good overlap of the hydrogen atomic orbitals. However, as the bond is stretched from its equilibrium position the overlap of the atomic orbitals decreases. As the atomic orbitals become more weakly coupled, they can no longer be properly interpreted as a molecular orbital. For twisted ethylene, also proposed by Mulliken,[14] and popularized by Salem and Turro,[15] the situation is very similar. As one side of the molecule is twisted with respect to the other, the overlap of the atomic p orbitals that form the π bond decreases (the bond is fully ruptured at a twist angle of 90°). For both of these cases, the four electronic states that arise (three singlet states and a triplet state) from two electrons in two orbitals can be represented as a pair of diradical states and a pair of zwitterionic states. The diradical like states are the fully occupied bonding orbital and the triplet state with one electron in the bonding orbital and one in the antibonding orbital with their spins parallel. The zwitterionic states consist of the singlet state with one electron in the bonding orbital and one in the antibonding orbital with their spins antiparallel and the doubly occupied antibonding orbital. While no direct evidence for this manifold has been provided for hydrogen, this manifold has been observed in the photoreactions of substituted ethylenes and other alkenes that undergo *cis-trans* isomerization.[16] The first spectroscopic evidence for the existence of twisted ethylene was provided by Ziegler and Hudson in their resonance Raman study of ethylene.[17] Recently, as pulsed lasers have become faster, there has been a resurgence in the effort to quantitate the excited states of twisted ethylene and some indirect spectroscopic evidence

for the existence of ionic excited states has been obtained from time-resolved spectroscopy.[18]

Due to the poor coupling of the atomic orbitals that form the δ bond, it too can be represented with the same collection of electronic states. It is quite ironic that a similar situation exists in inorganic chemistry, and even more that it exists in quadruply bonded metal dimers that possess the shortest bonds in inorganic chemistry.

In order to better understand the electronic states of the δ manifold (and, for that matter, the π manifold for twisted ethylene and the σ manifold for stretched hydrogen), it is useful to investigate the two limits of bond formation. At one extreme, where the atomic orbitals are strongly overlapped, the molecular orbital model is valid. At the other extreme, the weak coupling limit, the valence bond model is preferred. The inadequacy of the molecular orbital model is revealed when the δ bonds are derived. In the molecular orbital model, the orbitals are written as a linear combination of atomic orbitals (LCAO-MO). The simple linear combinations of atomic d_{xy} orbitals on metals A and B are:[19]

$$\delta_1 = [d_{xy}(A) + d_{xy}(B)] \equiv \delta \tag{I.2a}$$

$$\delta_2 = [d_{xy}(A) - d_{xy}(B)] \equiv \delta^* \tag{I.2b}$$

The doubly occupied ground state (δ^2) and excited state (δ^{*2}) are then given by:

$$\delta_1^2 = \left[d_{xy}(A) d_{xy}(B) + d_{xy}(B) d_{xy}(A) \right]^{\text{covalent terms}} + \left[d_{xy}(A) d_{xy}(A) + d_{xy}(B) d_{xy}(B) \right]^{\text{ionic terms}} \equiv \delta_{MO}^2 \tag{I.3a}$$

$$\delta_2^2 = \left[d_{xy}(A) d_{xy}(A) + d_{xy}(B) d_{xy}(B) \right]^{\text{ionic terms}} - \left[d_{xy}(B) d_{xy}(A) + d_{xy}(A) d_{xy}(B) \right]^{\text{covalent terms}} \equiv \delta_{MO}^{*2} \tag{I.3b}$$

It can readily be seen that the molecular orbital model predicts an equal probability for the electrons to be associated with separate atoms as it does for the electrons to be near the same atom.[20] A direct consequence of this is that upon dissociation the fragments are as likely to be neutral as ionic.

The valence bond (VB) model represents the opposite extreme in bond formation. In this model, the electrons are assumed to remain associated with their "correct" nucleus, the result of this is a purely covalent description of the bond:

$$\delta_I^2 = d_{xy}(A)d_{xy}(B) + d_{xy}(B)d_{xy}(A) \equiv \delta_{VB}^2 \qquad (I.4)$$

When the energies of the two extremes (LCAO-MO and VB) are plotted as a function of internuclear separation, R (or orbital overlap, S), and compared with a realistic Morse type potential (Figure 1.3), the difference between the two models becomes obvious. The LCAO-MO method is a sound approximation when the parent orbitals are strongly coupled at short R or large S. However, as the bond is broken, the orbitals become weakly coupled and the LCAO method fails to predict the proper dissociation energy because the molecule has an equal probability of forming ions as compared to neutrals. The VB model, on the other hand, properly predicts the dissociation of the molecule to neutrals in the weak coupling limit since it assumes the electrons remain associated with a particular nucleus, but fails to properly predict the energy when the orbitals are strongly coupled because it ignores the favorable attraction between ions.

These two methods do converge. In the valence bond model this is done by allowing a certain amount of ionic character to be built into the wavefunction:[19]

$$\delta_I^2 = d_{xy}(A)d_{xy}(B) + d_{xy}(B)d_{xy}(A)$$
$$+\lambda\left[d_{xy}(A)d_{xy}(A) + d_{xy}(B)d_{xy}(B)\right] \equiv \delta^2 \qquad (I.5)$$

where λ is referred to as the ionicity. The LCAO-MO model requires a more subtle approach.[19] To do this, the states that arise from placing two electrons into two orbitals

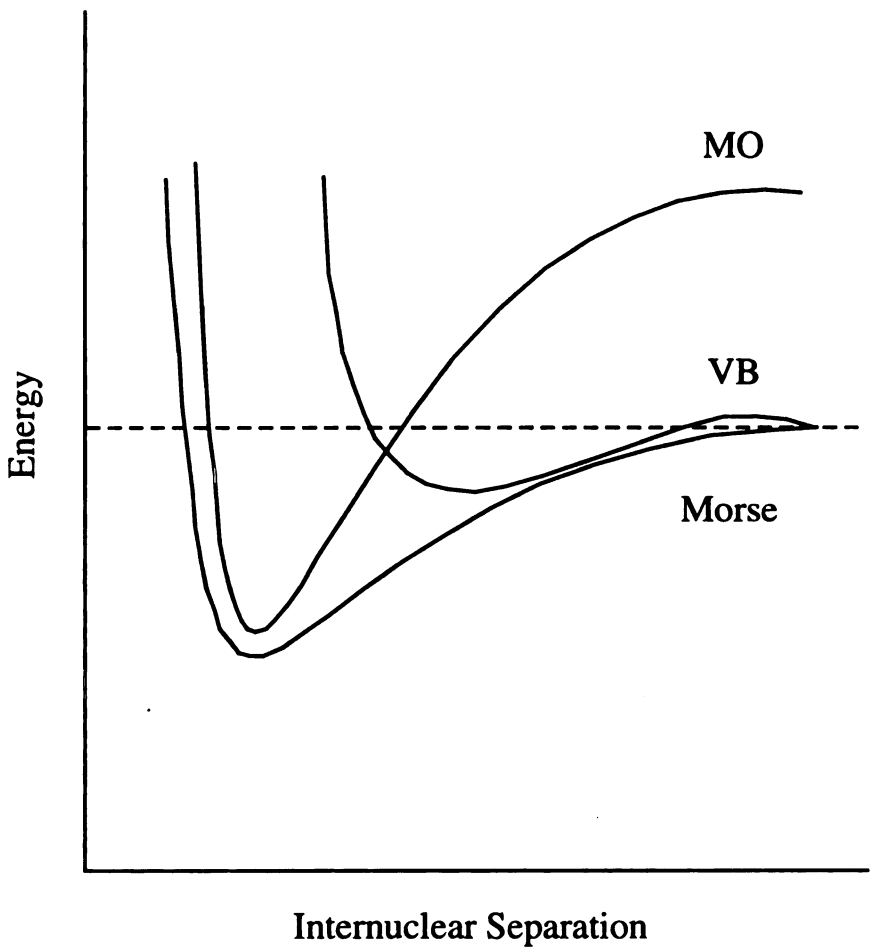

Figure I.2. Qualitative comparison of the energies obtained from the molecular orbital (MO) model, the valence bond (VB) model, and a realistic Morse type potential. These energies are representative of those obtained for the hydrogen molecule in Reference 20

must be considered. There are four possible states to be considered, along with their symmetries (in the D_{4h} point group). The first is the doubly occupied ground state δ^2 (A_{1g}). Two states can be formed by the promotion of one electron to the antibonding orbital, $^3\delta\delta^*$ and $^1\delta\delta^*$ ($^{3,1}A_{2u}$). The fourth state is the doubly occupied antibonding state δ^{*2} (2^1A_{1g}). The wavefunctions for each of these states, including their spin functions (ignoring normalization) are:[21]

$$\delta^2=\delta_1(1)\delta_1(2)\{\alpha_1\beta_2-\beta_1\alpha_2\}:{}^1A_{1g} \quad \text{(I.6a)}$$

$$^3\delta\delta^*=\{\delta_1(1)\delta_2(2)-\delta_2(1)\delta_1(2)\}\{\alpha_1\beta_2+\beta_1\alpha_2\}:{}^3A_{2u} \quad \text{(I.6b)}$$

$$^1\delta\delta^*=\{\delta_1(1)\delta_2(2)+\delta_2(1)\delta_1(2)\}\{\alpha_1\beta_2-\beta_1\alpha_2\}:{}^1A_{2u} \quad \text{(I.6c)}$$

$$\delta^{*2}=\delta_2(1)\delta_2(2)\{\alpha_1\beta_2-\beta_1\alpha_2\}:2^1A_{1g} \quad \text{(I.6d)}$$

where 1 and 2 are electron labels, α and β are spin functions for the electrons and δ_1 and δ_2 represent the bonding molecular orbital and antibonding molecular orbital described by the LCAO model above (Equations I.2a and I.2b).

To adjust the LCAO model to more correctly describe the actual system, the interaction between states of the same symmetry must be considered (so-called configuration interaction (CI)). The effect of configuration interaction can be seen by allowing the Hamiltonian, which is a totally symmetric function (A_{1g} in the D_{4h} point group), to act on the states of like symmetry (the two $^1A_{1g}$ states). The matrix elements for this interaction are given by $\langle {}^1A_{1g}|\mathbf{H}|2^1A_{1g}\rangle = {}^1A_{1g}$. This interaction between the states is repulsive and forms the basis for the non-crossing rule of states of like symmetry.[19] As a result, the doubly occupied ground state wavefunction (δ^2) and excited state wave function (δ^{*2}) are better represented by:

$$^1A_{1g}=C_1\delta^2+C_1'\delta^{*2} \quad \text{(I.7a)}$$

$$2^1A_{1g}=C_2\delta^2+C_2'\delta^{*2} \quad \text{(I.7b)}$$

where C_i and C_i' are coefficients which represent the weighting of each wavefunction ($C_i^2 + C_i'^2 = 1$). As C_i approaches C_i' ($= 1/\sqrt{2}$) the wavefunctions become those given in the

LCAO model. This representation can be easily interpreted in the VB picture also; then C_1 represents the covalent character of the ground state and C_1' represents the ionic character. With these wave functions, it is possible to determine the relative energy of each state in the δ manifold.

The Hamiltonian for the total energy of the system ($\mathbf{H}_T$) consists of a Hamiltonian for each of the electrons ($\mathbf{H}^{(1)}$ and $\mathbf{H}^{(2)}$) and a $1/\mathbf{r}_{12}$ operator that describes the interactions (electron correlation effects) between the two electrons:[22]

$$\mathbf{H}_T=\mathbf{H}^{(1)}+\mathbf{H}^{(2)}+\frac{1}{\mathbf{r}_{12}} \qquad \text{(I.8)}$$

where $\mathbf{H}^{(i)}$ takes the form of a typical one electron Hamiltonian:[19]

$$\mathbf{H}^{(i)}=-\left(\frac{\hbar^2}{2m_e}\right)\nabla^2+V \qquad \text{(I.9)}$$

and V is the potential energy for the interaction between the electron and the nucleus.

$\mathbf{H}_T$ can be employed to calculate the energies of each of the states (including configuration interaction). The energies of the states (for a complete derivation, see Appendix I) are given by:[10]

$$E_{\delta^2}=C_1^2\{2W_1+J_{11}\}+C_1C_1'K_{12} \qquad \text{(I.10a)}$$

$$E_{^3\delta\delta^*}=W_1+W_2+J_{12}-K_{12} \qquad \text{(I.10b)}$$

$$E_{^1\delta\delta^*}=W_1+W_2+J_{12}+K_{12} \qquad \text{(I.10c)}$$

$$E_{\delta^{*2}}=C_2^2\{2W_2+J_{22}\}+C_2C_2'K_{12} \qquad \text{(I.10d)}$$

where W_i represents the energy of an electron in orbital i (the one-electron energy of the orbital). J_{ij} is the Coulomb repulsion of two electrons in the same orbital (i = j) or two electrons in different orbitals ($i \neq j$). K_{12} is the exchange energy, and is a measure of the energy required to move an electron from one metal center to another.

If there is no overlap of atomic orbitals (complete neglect of differential overlap (CNDO) approximation), then $J_{11} = J_{22} = J_{12}$. This allows the J terms to be neglected as a

constant offset in energy. Taking the average energy of the molecular orbitals (δ and δ*) as a reference point ($1/2\{W_1 + W_2\} = 0$), and setting $\Delta W = W_2 - W_1$ simplifies the energy expressions a great deal:

$$E_{\delta^2} = -\sqrt{K_{12}^2 + \Delta W^2} \quad \text{(I.11a)}$$

$$E_{^3\delta\delta^*} = -K_{12} \quad \text{(I.11b)}$$

$$E_{^1\delta\delta^*} = +K_{12} \quad \text{(I.11c)}$$

$$E_{\delta^{*2}} = +\sqrt{K_{12}^2 + \Delta W^2} \quad \text{(I.11d)}$$

These energies are plotted as a function of internuclear separation (or orbital overlap) in Figure I.3.[10] The left side of the figure represents a typical bonding situation where there is a great deal of overlap of the atomic orbitals, leading to $\Delta W >> K$. The exchange energy can be ignored in this situation and the total energy is approximated by sum of the one-electron energies. In other words, the energy is given by the LCAO model. It should be mentioned, however, that at this limit, the CNDO approximation is less valid so the electronic states are not necessarily symmetrically disposed. The right side represents the opposite extreme. There is very little overlap of the atomic orbitals that results in $\Delta W \sim 0$, and K, the two-electron exchange energy, dominates the energy. At this extreme, the ground state is described by a purely covalent wavefunction, and the doubly excited state by a purely ionic wavefunction.

I.B. Electronic Spectroscopy of Quadruply Bonded Metal-Metal Complexes

The most studied transition of quadruply bonded metal (M—4— M) dimers is the $^1\delta^2 \rightarrow {}^1\delta\delta^*$ ($^1(\delta \rightarrow \delta^*)$) transition. This transition has provided the basis for using the VB approach to interpret the electronic states of the δ manifold. The paradigm system, as mentioned in the Introduction (I.A), is $Re_2Cl_8^{2-}$. There are, however, many compounds that contain quadruple bonds. One particular class of compounds, those with the empirical formula $M_2X_4L_4$ (M = Mo or W; X = Cl, Br, or I, and L = monodentate P or As

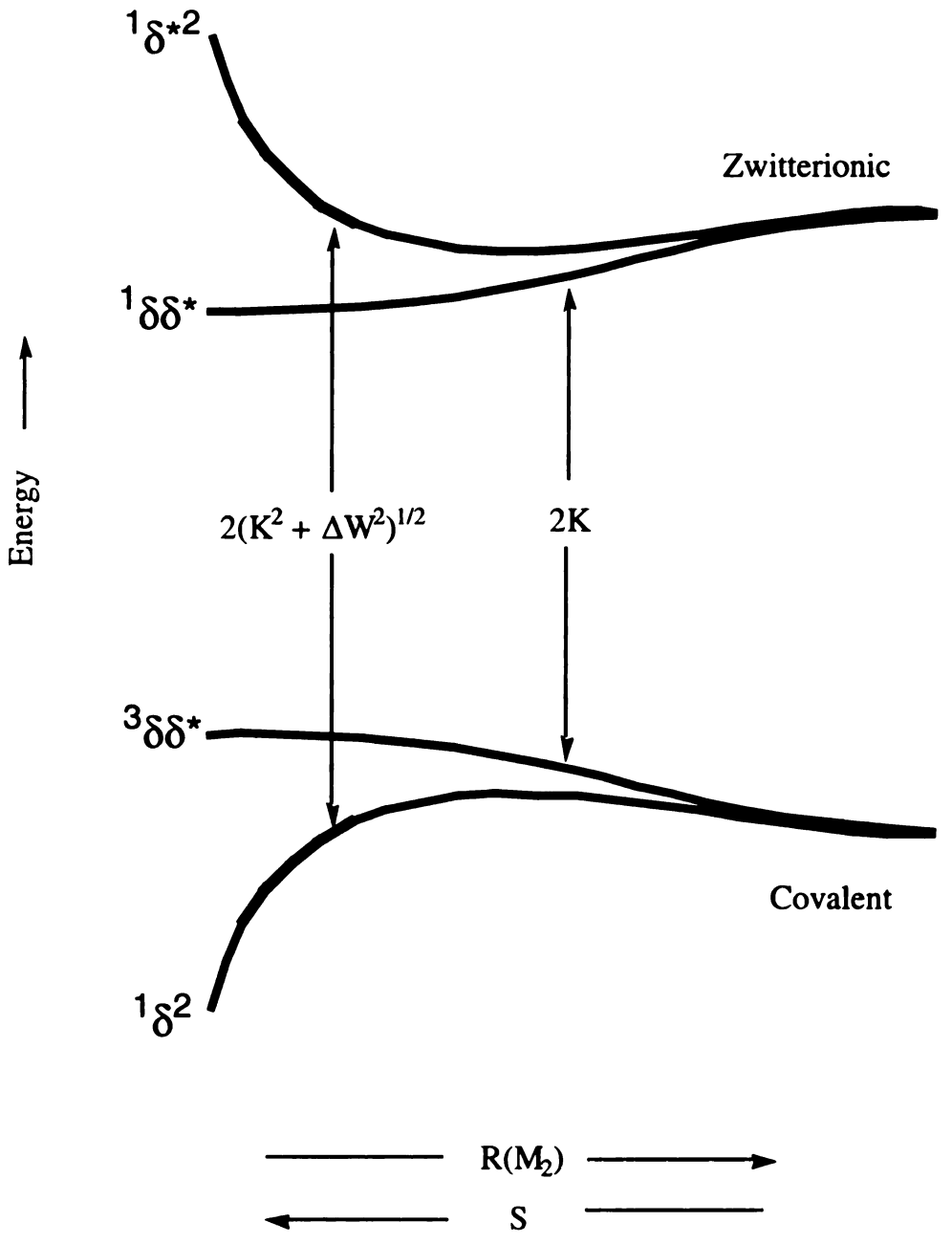

Figure I.3. Behavior of the electronic states of the δ-manifold as a function of orbital overlap (S) or internuclear separation (R).

ligand), has also been studied a great deal. Although these molecules are not as highly symmetric as $Re_2Cl_8^{2-}$ (D_{4h}), the reduction in symmetry to D_{2d}, while it has some effect on the MO diagram (Figure I.4), has no effect on the resultant energies of the electronic states of the δ manifold.

I.B.1. $Mo_2X_4(PR_3)_4$ Complexes

Of particular interest, in the context of this thesis, is the molecule in which X = Cl and R = Me. There are three prominent bands in the absorption spectrum of $Mo_2Cl_4(PMe_3)_4$ (Figure I.5). Each of the bands has been assigned in the literature[23,24] using polarized, single crystal spectroscopy. The highest energy band (λ_{max} = 325 nm, ε_{max} = 3720), is very strongly polarized perpendicular to the Mo—Mo (z) axis.[24] When the crystal is irradiated parallel to the axis at low temperatures the intensity of this band is very weak, which indicates the parallel component is possibly due to vibronic coupling. The strong perpendicular component is consistent with the band being assigned as the ligand-to-metal charge transfer (LMCT), $\sigma(MP) \rightarrow \delta^*$.[24] Here MP indicates association with the phosphine ligand. The next band is quite weak (λ_{max} = 435 nm, ε_{max} = 210).[24] The absorption appears in both parallel and perpendicular polarizations; however, the temperature dependence of the band is significantly different in each polarization. Under perpendicular polarization, the band sharpens and its intensity increases as the sample is cooled, which indicates the transition is dipole allowed. In parallel polarization, however, the intensity decreases with decreasing temperature suggesting the parallel component is vibronically induced. Since the perpendicular component is dipole allowed, the likely assignment of this absorption is metal-to-metal charge transfer (MMCT) $^1(\pi \rightarrow \delta^*)$;[24] the low intensity is attributable to the fact that this transition correlates with a dipole forbidden transition in D_{4h} symmetry.[24] The lowest energy band (λ_{max} = 585 nm, ε_{max} = 3110) is almost exclusively parallel polarized.[24] The ratio of the intensity of the parallel component to the

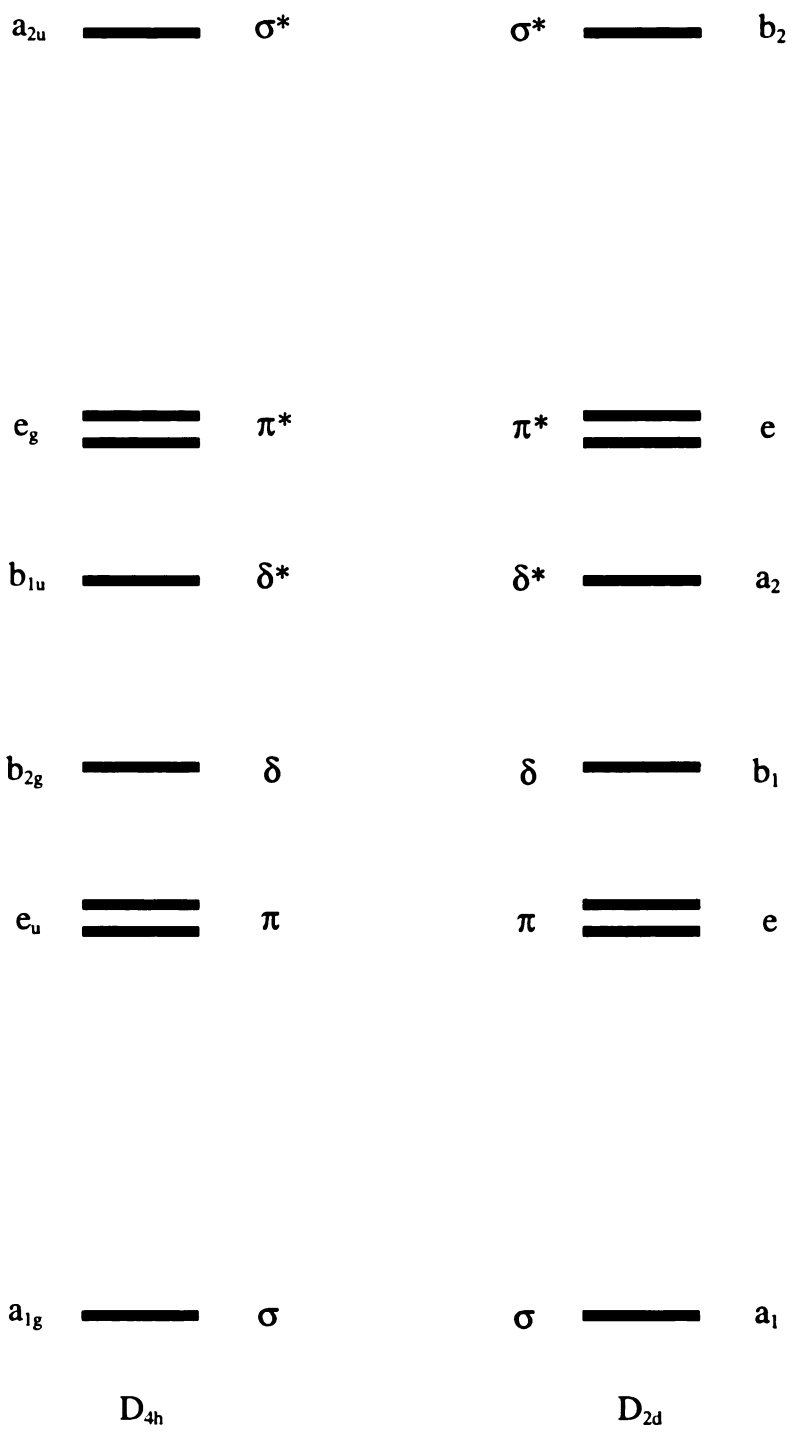

Figure I.4. Molecular orbital correlation diagram between D_{4h} and D_{2d} symmetries.

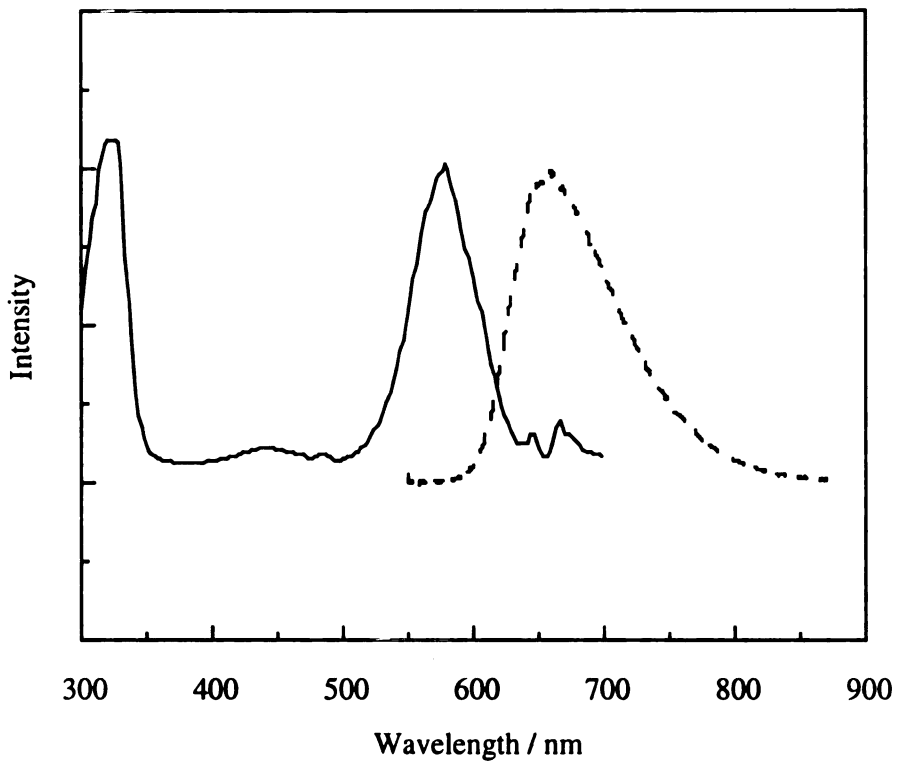

Figure I.5. Solution phase (3-methylpentane) electronic absorption (——) and emission (------) spectra of $Mo_2Cl_4(PMe_3)_4$

perpendicular component is nearly 100. At low temperature, the perpendicular component progresses with a spacing of ~340 cm^{-1},[24] consistent with the excited state $\nu_1(Mo_2)$ stretch (ground state $\nu_1(Mo_2)$ = 355 cm^{-1}),[23] leading to the assignment of this band as the MMCT $^1(\delta \rightarrow \delta^*)$.[24]

As shown in Figure I.5, $Mo_2Cl_4(PMe_3)_4$ is emissive ($\lambda_{max,em}$ = 673 nm; τ = 140 ns in 2-methylpentane, ϕ_{em} = 0.26).[25] Since the emission spectrum overlaps with the $^1(\delta \rightarrow \delta^*)$ absorption band, it is apparent that the fluorescence originates from the $^1\delta\delta^*$ state.[25] This is further supported by low temperature emission studies of the molecule dissolved in a 2-methylpentane glass. The band progresses with a spacing of 335 cm^{-1}, consistent with the ground state $\nu_1(Mo_2)$. Fluorescence excitation spectroscopy has also been performed on this molecule[26] and the excitation spectrum is shown in Figure I.6. The bands in the excitation spectrum mirror those in the absorption spectrum (since all of the bands in the absorption spectrum populate the δ^* orbital), and are assigned to the same states.

I.B.2. cis-$Mo_2Cl_2(mhp)_2(PMe_2Ph)_2$ Complexes

Replacement of two Cl^-s and two PMe_3s in $Mo_2Cl_4(PMe_3)_4$ with two bidentate mhp ligands (mhp = deprotonated 6-methyl-2-hydroxypyridine) also produces very emissive complexes ($\lambda_{max,em}$ = 602 nm; τ = 45 ns in *n*-hexane;[27] ϕ_{em} = 0.2[28]). The excitation and emission spectra of *cis*-$Mo_2Cl_2(mhp)_2(PMe_2Ph)_2$ [PMe_2Ph = dimethylphenylphosphine] are shown in Figure I.7. This molecule is not as symmetric as $Mo_2Cl_4(PMe_3)_4$ (C_2 *vs.* D_{2d}), which makes spectroscopic assignment more difficult since transitions are more readily vibronically induced. The spectroscopy of this compound has not been rigorously investigated. However, by comparison with the absorption and emission spectra of the closely related molecules $Mo_2Cl_2(mhp)_2(PEt_2Ph)_2$,[29] $Mo_2(mhp)_4$[30] and $Mo_2Cl_4(PMe_3)_4$,[23,24] which have been reported in the literature, reasonable assignments can be made. The maximum in the excitation spectrum at 550

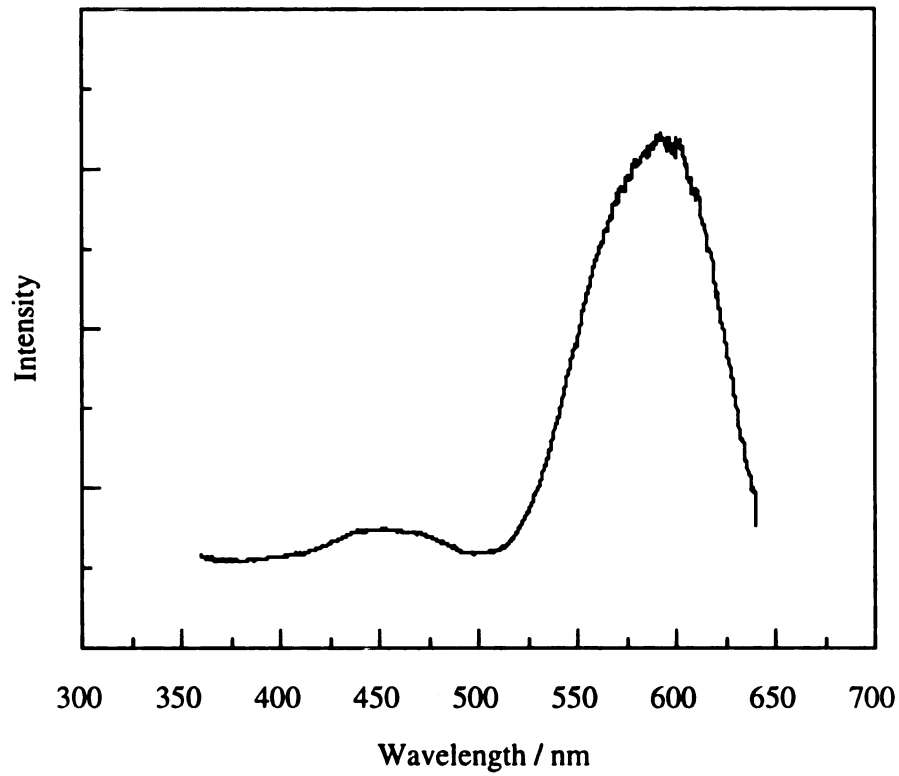

Figure I.6. Fluorescence excitation spectrum of $Mo_2Cl_4(PMe_3)_4$ in 3-methylpentane

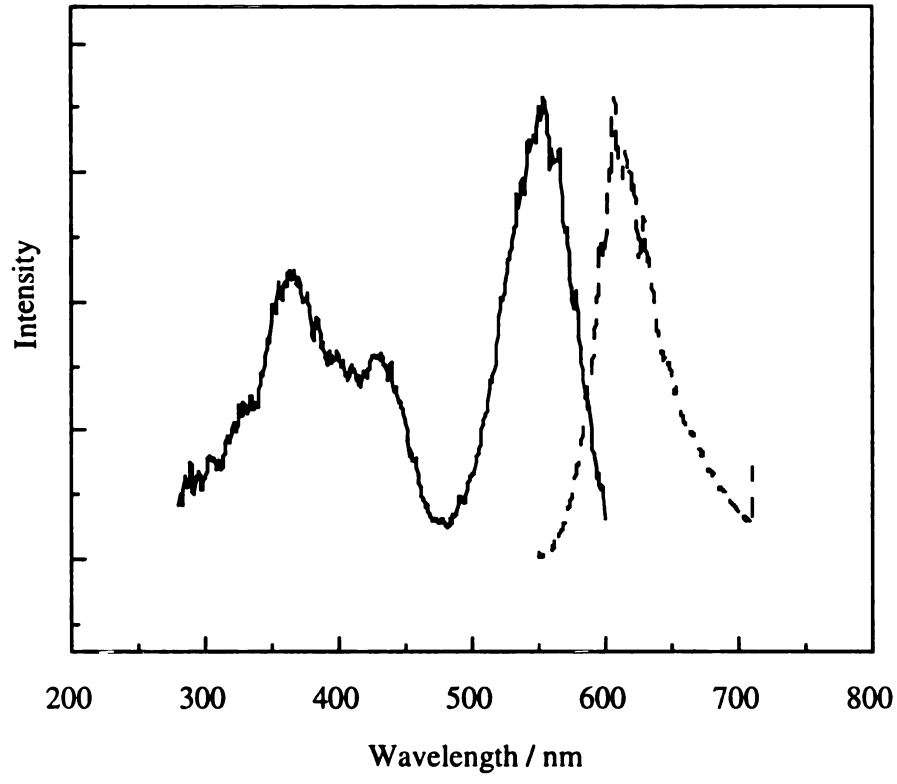

Figure I.7. Fluorescence excitation (——) and emission (------) spectra of *cis*-$Mo_2Cl_2(mhp)_2(PMe2Ph)_2$

nm is assigned as $^1(\delta \rightarrow \delta^*)$, the maximum at 440 nm is $^1(\pi \rightarrow \delta^*)$, but may contain some ligand based components through vibronic coupling; the maximum at 370 nm is assigned as a purely ligand-based transition. Since the emission band overlaps the $^1(\delta \rightarrow \delta^*)$ transition, the emission band originates from the $\delta\delta^*$ excited state.

I.C. Two Photon Spectroscopy

Perhaps one of the most often referred to equations in chemistry is Beer's Law (Beer-Lambert Law):[31]

$$A=\varepsilon b c \tag{I.12}$$

where A is the absorbance of the sample, ε is the molar absorptivity, b is the path length, and c is the concentration of the sample. Beer's law can be easily recast into a form which relates the intensity of radiation after the sample (I_f) to the intensity incident upon the sample (I_0):[31]

$$I_f=I_0 e^{-\alpha bc} \tag{I.13}$$

where α is the absorption coefficient and is related to the extinction coefficient by:[19]

$$\varepsilon=\frac{\alpha}{\ln 10} \tag{I.14}$$

It is ε (or α), then, which carries the quantum mechanical information about the molecule *via* the oscillator strength (f):[32]

$$f=\frac{4m_e c\varepsilon_0 \ln 10}{N_A e^2}\int \varepsilon(\nu)d\nu=\frac{8\pi^2}{3}\frac{m_e \nu}{he^2}\left|\mu_{fi}\right|^2 \tag{I.15}$$

where μ_{fi} is the transition dipole between the initial and final state (ψ_i and ψ_f):

$$\mu_{fi}=\int \psi_f^* \mu \psi_i \; ; \mu = e\mathbf{r} \tag{I.16}$$

Another fundamental property of a molecule, the refractive index (n) can also be obtained from Beer's law. The refractive index is a measure of how much light slows

down (the phase is changed) as it passes through a material (Figure I.8). The electric field of the radiation (E(z,t)) at a point much behind the sample (z>>b) is given by:[33]

$$E(z,t)=e^{\{i\omega(n-1)b/c\}}E_0e^{\{-i\omega(t-z/c)\}} \qquad (I.17)$$

where z is the direction of propagation of the field, b is the sample thickness (Figure I.8) c is the speed of light, E_0 is the unperturbed electric field amplitude and ω is the angular frequency of the radiation ($\omega = 2\pi\nu$). The first term is often referred to as the phase factor and for $n-1 < 1$ can be expanded as:[33]

$$E(z,t)=[1+i\omega(n-1)b/c+....]E_0e^{\{-i\omega(t-z/c)\}} \qquad (I.18)$$

One can assume that the dipole can be approximated by an electron (charge q) attached to an infinitely heavy mass (nucleus). When an oscillating electric field ($E_0e^{-i\omega t}$) is applied to the dipole it behaves as a driven, damped (through reradiation of the incident electromagnetic field) harmonic oscillator. The equation of motion for the dipole in one dimension (x) is then:[34]

$$m\ddot{x}+\gamma\dot{x}+kx=E_0e^{-i\omega t} \qquad (I.19)$$

where m is the mass of the electron, γ is the damping constant, and k is the restoring force ($k = m_e\omega_0^2$, ω_0 is the angular frequency of the oscillator). The trajectory of the electron, x(t), is then:

$$x(t)=\frac{(q/m)E_0e^{-i\omega t}}{\omega_0^2-\omega^2-i\omega c} \qquad (I.20)$$

All of the dipoles following this trajectory reradiate electromagnetic energy at frequency ω and have a strong resonance (absorption) at $\omega = \omega_0$. The total field at some distance away from the sample is then the sum of unaffected electric field, plus the field that is phase shifted:[33]

$$E(z,t)=E_0e^{-i\omega(t-z/c)}\left(1+\frac{bq^2N\omega}{2\varepsilon_0cm(\omega_0^2-\omega^2-i\omega\gamma)}\right) \qquad (I.21)$$

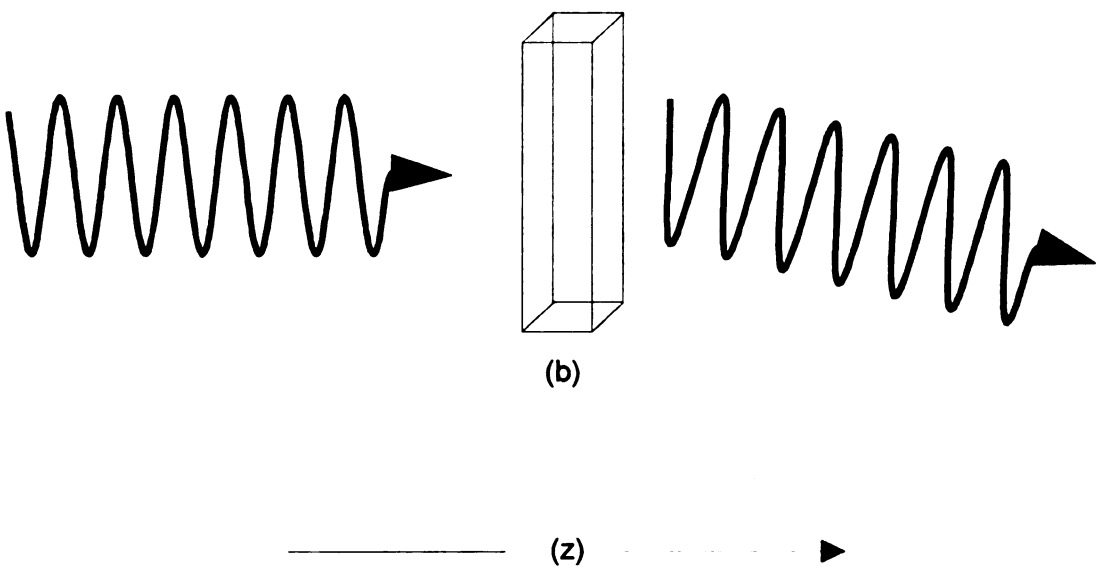

Figure I.8. The effect of refractive index on an oscillating electric field propagating in the z direction. b is the sample thickness.

where N is the number of dipoles and ε_0 is the permitivity of free space. Equating this expression for the field with Equation I.18 above allows n to be determined:

$$n=1+A(\omega_0;\omega)\left[\omega_0^2-\omega^2+i\omega\gamma\right] \qquad (I.22)$$

where $A(\omega_0;\omega) = Nq^2/2\varepsilon_0 m_e[(\omega_0^2-\omega^2)^2 + \gamma^2\omega^2]$. This demonstrates that the refractive index is a complex number that can be written as:

$$n=Re(n)+i\,Im(n) \qquad (I.23)$$

where the real and imaginary parts are given by:

$$Re(n)=1+A(\omega_0;\omega)(\omega_0^2-\omega^2) \qquad (I.24a)$$

$$Im(n)=\gamma\omega A(\omega_0;\omega) \qquad (I.24b)$$

When this index of refraction is substituted into the phase shift term (Equation I.18) and the resultant electric field is squared, the intensity at a point after the sample is given by:[35]

$$I(z)=\frac{E(z,t)^* E(z,t)c\varepsilon_0}{2} \qquad (I.25)$$

Similarly, I_0 can be determined from E_0. A different expression for Beer's law is found, this time dependent on the imaginary part of the refractive index:

$$I(z)=I_0 e^{-2\omega Im(n)b/c} \qquad (I.26)$$

Therefore, the refractive index serves two roles; the real part imparts a phase shift onto the incident beam, and the imaginary part (the absorption coefficient) serves to attenuate the beam.

A second way to look at refraction and absorption is through the relationship between the average dipole moment density (**P**) which is induced in the sample by the driving electromagnetic field (**E**):[36]

$$\mathbf{P}=\chi\mathbf{E} \qquad (I.27)$$

The incident electric field is attenuated and phase shifted by χ, the susceptibility of the material. It has been shown that χ is related to the refractive index:[36]

$$n^2=1+4\pi\chi \tag{I.28}$$

The susceptibility has both imaginary and real components, just as the refractive index does:

$$\chi=\mathrm{Re}(\chi)+i\,\mathrm{Im}(\chi) \tag{I.29}$$

where the real part serves to retard the phase of the incident electric field, and the imaginary part attenuates the electric field. The real and imaginary components of χ in terms of the refractive index are then:[33]

$$\mathrm{Re}(\chi)=\frac{\mathrm{Re}(n)^2-\mathrm{Im}(n)^2-1}{4\pi} \tag{I.30a}$$

$$\mathrm{Im}(\chi)=\frac{\mathrm{Re}(n)\,\mathrm{Im}(n)}{2\pi} \tag{I.30b}$$

Therefore, Beer's law can also be written in terms of the susceptibility:

$$I_f=I_0e^{-4\pi\,\mathrm{Im}(\chi)b/c\,\mathrm{Re}(n)} \tag{I.31}$$

To this point, the dipole has been assumed to behave linearly as a harmonic oscillator responding to a harmonic driving force. However, as the driving force becomes more intense, the dipole can no longer respond linearly (either the electron is ejected, or the oscillator becomes overdriven), this results in a nonlinear response as the dipole becomes anharmonic. This anharmonicity is treated by expanding the susceptibility as a power series:[33]

$$\mathbf{P}=\left(\chi^{(1)}+\chi^{(2)}\mathbf{E}+\chi^{(3)}\mathbf{E}^2+\ldots\right)\mathbf{E} \tag{I.32}$$

These higher order susceptibilities give rise to nonlinear responses to the driving force, which are well known in optics. Second harmonic generation, where two frequencies are mixed to form a third frequency that is the sum of the original two frequencies, arises from $\chi^{(2)}$ (Figure I.9). Sum frequency generation is a common example where three

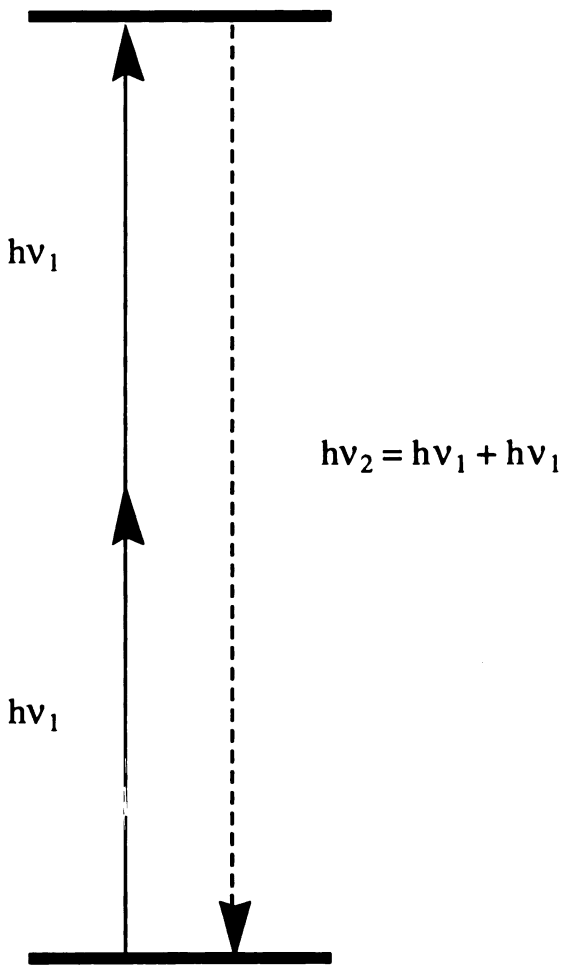

Figure I.9. Second Harmonic Generation. Two electric fields are mixed through the second order susceptibility tensor, $\chi^{(2)}$, to produce a third electric field.

frequencies are mixed through $\chi^{(3)}$ to generate a fourth frequency (Figure I.10). In addition to these optical effects, nonlinear responses to driving forces are also common in spectroscopy. Coherent anti-stokes Raman spectroscopy (CARS) and two-photon absorption spectroscopy are but two examples of four wave mixing through $\chi^{(3)}$ in spectroscopy (Figure I.11).

Two-photon spectroscopy has several characteristics that separate it from conventional, linear spectroscopy. The first is the difference in selection rules. Using two-photon techniques it is possible to observe states that are forbidden to conventional spectroscopy.[37] A second characteristic is the quadratic dependence of the observed signal on the incident electric field.[38] The third, and perhaps the most useful distinction, is the dependence of the two-photon transition probability on the polarization of the incident radiation.[39] Advantage can be taken of this characteristic to determine symmetry assignments of two-photon allowed excited states by appropriate choice of the experimental arrangement.

I.C.1. Selection Rules

The allowedness of a spectroscopic transition is governed by orbital, vibronic, and spin selection rules. The one most important to distinguish between one- and two-photon spectroscopy is the orbital or Laporte selection rule. The transition dipole, μ_{fi}, for a one-photon process is given by:[40]

$$\mu_{fi} = \langle \psi_f | \mu_j | \psi_i \rangle ; \mu = \mathbf{er} \qquad \text{(I.33)}$$

where ψ_f and ψ_i are wavefunctions representing the final and initial states respectively, and μ_j is the dipole moment in the j direction. From group theory, for a transition to have nonzero intensity, the product $\psi_f \mu_j \psi_i$ must be an even function (must include the totally symmetric irreducible representation). Since μ_j is an odd function that transforms as x, y, or z, the product of $\psi_f \psi_i$ must also be an odd function. For centrosymmetric systems this

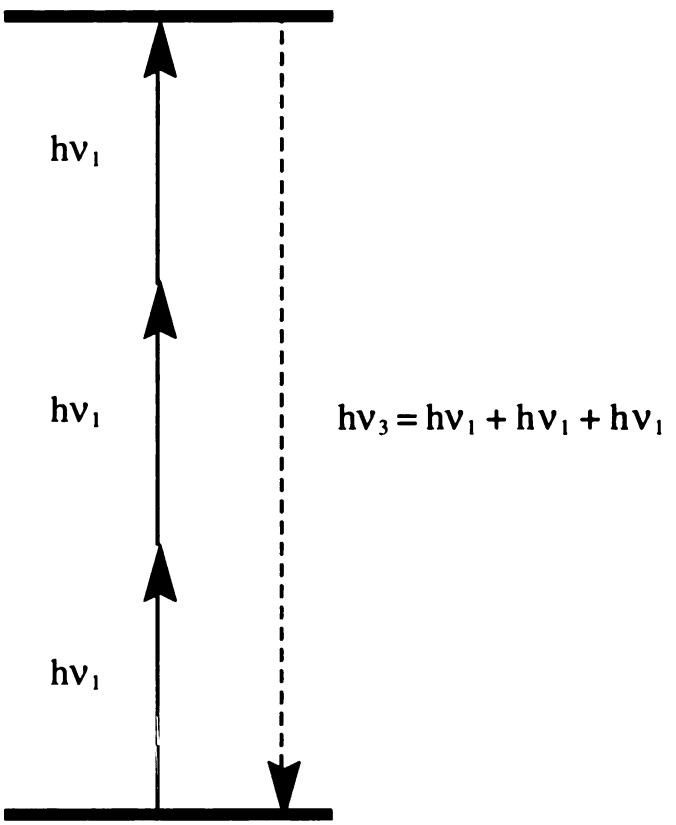

Figure I.10. Sum Frequency Generation (SFG). Three electric fields are mixed through the third order susceptibility tensor, $\chi^{(3)}$, to produce a fourth electric field.

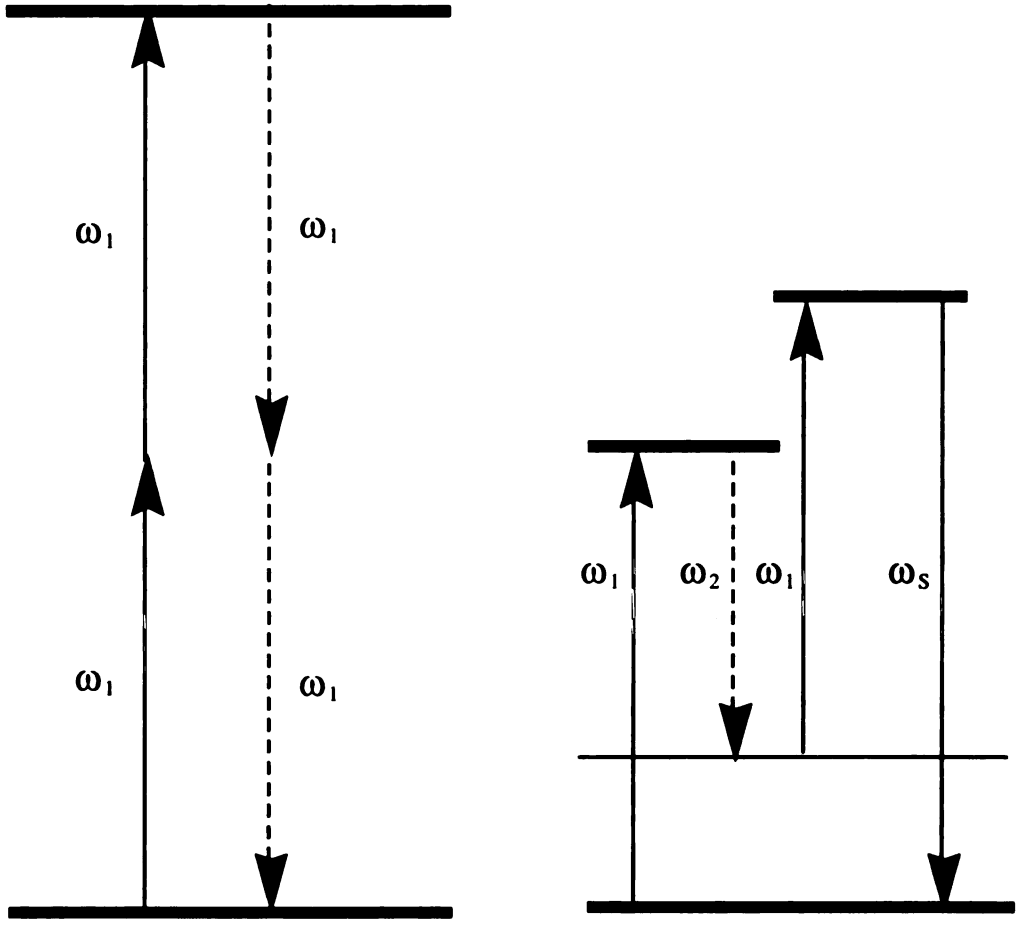

Figure I.11. Two examples of nonlinear spectroscopy. (a) Two-photon absorption (TPA) spectroscopy and (b) coherent anti-Stokes Raman spectroscopy (CARS).

results in g ↔ u transitions being allowed and g ↔ g or u ↔ u transitions being forbidden.

In two-photon spectroscopy, on the other hand, the allowedness of the transition is given by the two-photon transition tensor, S:[38a]

$$S \propto \left\langle \psi_f \left| \mu_j^{(1)} \right| \psi_n \right\rangle \left\langle \psi_n \left| \mu_l^{(2)} \right| \psi_i \right\rangle \qquad \text{(I.34)}$$

where ψ_n describes an intermediate state (that can be either real or virtual), and μ_j and μ_l indicates that the dipole moments involved in the transition need not necessarily be the same. The effective two-photon operator is then $\mu_j\mu_l$. The product of the two dipole moment operators transforms as x^2, y^2, z^2, xy, xz, or yz, all of which are even functions. Therefore, g ↔ g and u ↔ u transitions are allowed in two-photon spectroscopy and g ↔ u transitions are forbidden.

I.C.2. Power Dependence

The probability for a two-photon transition can be determined from time-dependent perturbation theory.[38a] When both photons involved in the transition are from the same laser ($\omega_1 = \omega_2 = \omega_r$), the transition probability, $W^{(2)}$, is given by:

$$W^{(2)} \propto I_0^2 \left| \sum_n \frac{\langle \psi_f | \mu | \psi_n \rangle \langle \psi_n | \mu | \psi_i \rangle}{\Delta E_{ni} - \hbar\omega_r} \right|^2 \qquad \text{(I.35)}$$

where I is the intensity of the incident laser beam, ψ_n represents the intermediate state and ψ_i and ψ_f are the initial and final state wavefunctions, respectively. ΔE_{ni} is the energy of the intermediate state and ω_r is the frequency of the incident radiation. This equation shows that the transition probability is proportional to the square of the intensity of the incident laser beam. In general, for any n-photon transition induced by a single source and below saturation, the probability it proportional to I^n. When a two-photon transition is saturated, the probability can be shown to be proportional to $I^{3/2}$.[38a] In general, quadratic dependence can be a powerful tool in determining if an observed

transition results from a two-photon absorption. Taking the logarithm of each side of equation (35) results in the more familiar expression:

$$\log W^{(2)} = 2\log I + \log C \qquad \text{(I.36)}$$

where the terms have the same meaning as before and C represents the terms in the summation along with experimental variables that are independent of the irradiation power.

I.C.3. Polarization Dependence

In linear spectroscopy the symmetry of an excited state can only be determined by using a rigidly oriented sample. In two-photon spectroscopy, however, excited state symmetries can be determined for randomly oriented samples. The role of polarization in two-photon spectroscopy was first investigated by Monson and McClain[39] and later by Nascimento.[41] This attribute has made two-photon spectroscopy a valuable tool to spectroscopists.

In one-photon spectroscopy the absorption cross-section, σ, for randomly oriented molecules is related to the transition dipole (defined in equation 33):

$$\sigma \propto \left|\lambda \cdot \mu_{fi}\right|^2 \qquad \text{(I.37)}$$

where λ is the unit polarization vector of the absorbed photon. Since $\lambda \cdot \lambda^* = 1$ there is no polarization information contained in the observed transition.

In two-photon spectroscopy, however, the cross-section, $\langle\delta\rangle$ (more correctly, the absorptivity), is given by:[39]

$$\langle\delta\rangle = \left|\lambda \cdot \mathbf{S}_{fi}^{ab} \cdot \kappa\right|^2 \qquad \text{(I.38)}$$

where κ and λ are the polarization vectors of the two absorbed photons and S_{fi}^{ab}, the two-photon transition tensor is:[39]

$$S_{fi}^{ab}=\sum_{n}\frac{\langle\psi_f^b|\mu|\psi_n^b\rangle\langle\psi_n^a|\mu|\psi_i^a\rangle}{\omega_{ni}-\omega_\kappa}+\frac{\langle\psi_f^a|\mu|\psi_n^a\rangle\langle\psi_n^b|\mu|\psi_i^b\rangle}{\omega_{ni}-\omega_\lambda} \qquad (I.39)$$

where ω_{ni} is the energy of the intermediate state and ω_j ($j = \kappa$ or λ) is the energy of the photon absorbed. The cross-section is most often written in terms of molecular parameters and polarization (experimental) parameters:[39]

$$\langle\delta\rangle=\delta_F F+\delta_G G+\delta_H H \qquad (I.40)$$

where, F, G, and H are functions of the polarization of the absorbed photons:

$$F=4|\lambda\cdot\kappa|^2-1-|\lambda\cdot\kappa^*|^2 \qquad (I.41a)$$

$$G=-|\lambda\cdot\kappa|^2+4-|\lambda\cdot\kappa^*|^2 \qquad (I.41b)$$

$$H=-|\lambda\cdot\kappa|^2-1+4|\lambda\cdot\kappa^*|^2 \qquad (I.41c)$$

and δ_F, δ_G and δ_H are functions of molecular parameters:

$$\delta_F\propto\sum_a\sum_b S_{fi}^{aa}S_{fi}^{bb*} \qquad (I.42a)$$

$$\delta_G\propto\sum_a\sum_b S_{fi}^{ba}S_{fi}^{ba*} \qquad (I.42b)$$

$$\delta_H\propto\sum_a\sum_b S_{fi}^{ba}S_{fi}^{ab*} \qquad (I.42c)$$

where a and b represent the molecular axes and S_{fi}^{aa} are the two-photon transition tensors as before. If two photons of the same energy are used then $\delta_G = \delta_H$ ($S^{ba} = S^{ab}$). Since δ_F is then the square of the trace of the tensor (which implies it is totally symmetric), it is only nonzero if the excited state is of the same symmetry as the ground state.

The values of F, G, and H have been calculated for the eight possible polarization cases[39] (using circularly and linearly polarized light) and are shown in Table I.2. The tensor patterns have also been determined[39,41] for most symmetries and the relevant

Table I.2. Values for the polarization functions F,G, and H, depending on the eight polarization cases. From References 37 and 39.

Case	1	2	3	4	5	6	7	8
	↑↑	↑→	↻↗	↻↺	↑↗	↑↺	↻↻	↻↺
F	2	-1	-1	-1/4	1/2	1/2	-2	3
G	2	4	4	7/2	3	3	3	3
H	2	-1	-1	-1/4	1/2	1/2	3	-2

Polarization Cases:

(1) Two linearly polarized photons with parallel polarization.

(2) Two linearly polarized photons with perpendicular polarization.

(3) One linear and one circular with the linear photon polarized such that it is perpendicular with the plane of the circularly polarized photon.

(4) Both circular with propagation opposite to each other.

(5) Both linear, with 45° between their polarization vectors.

(6) One linear and one circular with the linear photon polarized such that it is parallel with the plane of the circularly polarized photon.

(7) Two circularly polarized with polarization in the same sense.

(8) Two circularly polarized with polarization in the opposite sense.

patterns are shown in Table I.3 along with their polarization ratio, Ω, that is defined as:[38a]

$$\Omega = \frac{\langle \delta_{cir} \rangle}{\langle \delta_{lin} \rangle} \tag{I.43}$$

here $\langle \delta_{cir} \rangle$ and $\langle \delta_{lin} \rangle$ are the cross sections for using two circularly and two linearly polarized photons respectively and are given by:

$$\langle \delta_{cir} \rangle = F\delta_F + (G+H)\delta_G = -2\delta_F + 6\delta_G \tag{I.44a}$$

$$\langle \delta_{lin} \rangle = F\delta_F + (G+H)\delta_G = +2\delta_F + 4\delta_G \tag{I.44b}$$

where F, G, and H have been taken from Table I.2 (cases 7 and 1 for two circularly polarized photons and two linearly polarized photon respectively). The polarization ratio is bounded by:

$$0 \leq \Omega \leq \frac{3}{2} \tag{I.45}$$

Therefore, by measuring the intensity of a transition when two circularly polarized photons are used and comparing that to the intensity when two linearly polarized photons are used, the symmetry of the states involved in the transition can be determined.

I.D. Motivation

The applicability of the VB model would have significant ramifications on the potential photochemistry of these molecules. If the model provides a fair representation of the upper excited states of the δ manifold, then these states should undergo

Table I.3. Two-photon tensor patterns and the polarization ratio (Ω) expected for each transition in the D_{2d} and D_{4h} point groups. From References 37, 39, and 41.

Tensor Pattern operator	Transition Symmetry (gs $\leftrightarrow$ es)†	Polarization Ratio Ω
A_1: $x^2 + y^2, z^2$ $\begin{pmatrix} s_1 & 0 & 0 \\ 0 & s_1 & 0 \\ 0 & 0 & s_2 \end{pmatrix}$	$A_1 \leftrightarrow A_1$; $A_2 \leftrightarrow A_2$; $B_1 \leftrightarrow B_1$; $B_2 \leftrightarrow B_2$	$\Omega < 1$
B_1: $x^2 - y^2$ $\begin{pmatrix} s_3 & 0 & 0 \\ 0 & -s_3 & 0 \\ 0 & 0 & 0 \end{pmatrix}$	$A_1 \leftrightarrow B_1$ $A_2 \leftrightarrow B_2$	$\Omega = 3/2$
B_2: xy $\begin{pmatrix} 0 & s_4 & 0 \\ -s_4 & 0 & 0 \\ 0 & 0 & 0 \end{pmatrix}$	$A_1 \leftrightarrow B_2$ $A_2 \leftrightarrow B_1$	$\Omega = 3/2$
E: xz, yz $\begin{pmatrix} 0 & 0 & s_5 \\ 0 & 0 & -is_5 \\ s_6 & -is_6 & 0 \end{pmatrix}$ and $\begin{pmatrix} 0 & 0 & s_5^* \\ 0 & 0 & -is_5^* \\ s_6^* & -is_6^* & 0 \end{pmatrix}$	$A_1 \leftrightarrow E$ $E \leftrightarrow E$	$\Omega = 3/2$

† gs = ground state symmetry; es = excited state symmetry.

unprecedented multielectron chemistry due to the ionic nature of the excited states ($^{+}$M—M:$^{-}$). Multielectron photochemistry has already been observed from these states in the oxidative addition of CH_3I to $W_2Cl_4(dppm)_2$:[42]

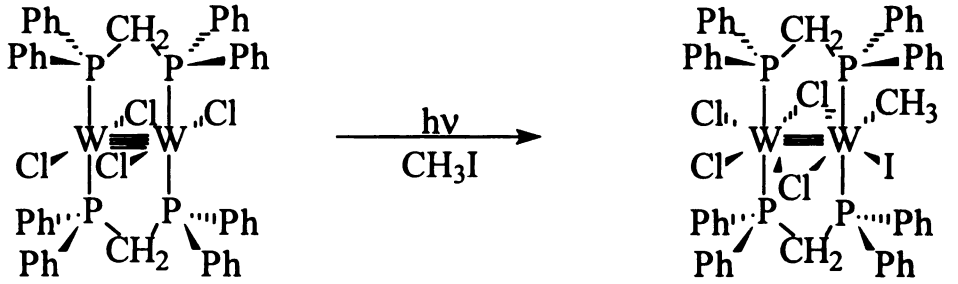

This reaction has been shown to proceed upon excitation of the $^1(\pi \rightarrow \delta^*)$ transition. It is presumed that it is necessary to excite this transition to provide a weakened π bond involving the Cl^- ligands, which then allows the Cl^- ligands to fold over to an edge-sharing bioctahedral arrangement, thus providing a vacant coordination site on the reduced metal center:[43]

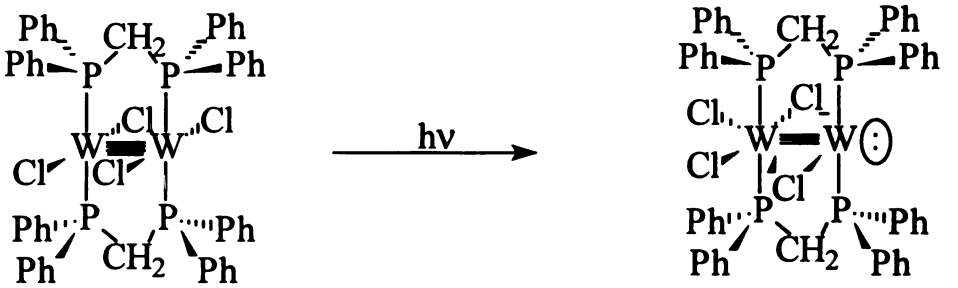

The product species has been observed in nanosecond transient absorption studies (τ > 100 μs) (Figure I.12a)[43,44]. The spectrum of the transient species is consistent with the spectra of the edge-sharing bioctahedral analogs $W_2Cl_6(PEt_3)_4$ and $W_2Cl_6(dppm)_2$ (Figure I.12b). This mechanism is plausible in the context of the VB model where ionic excited states are presumed to exist.

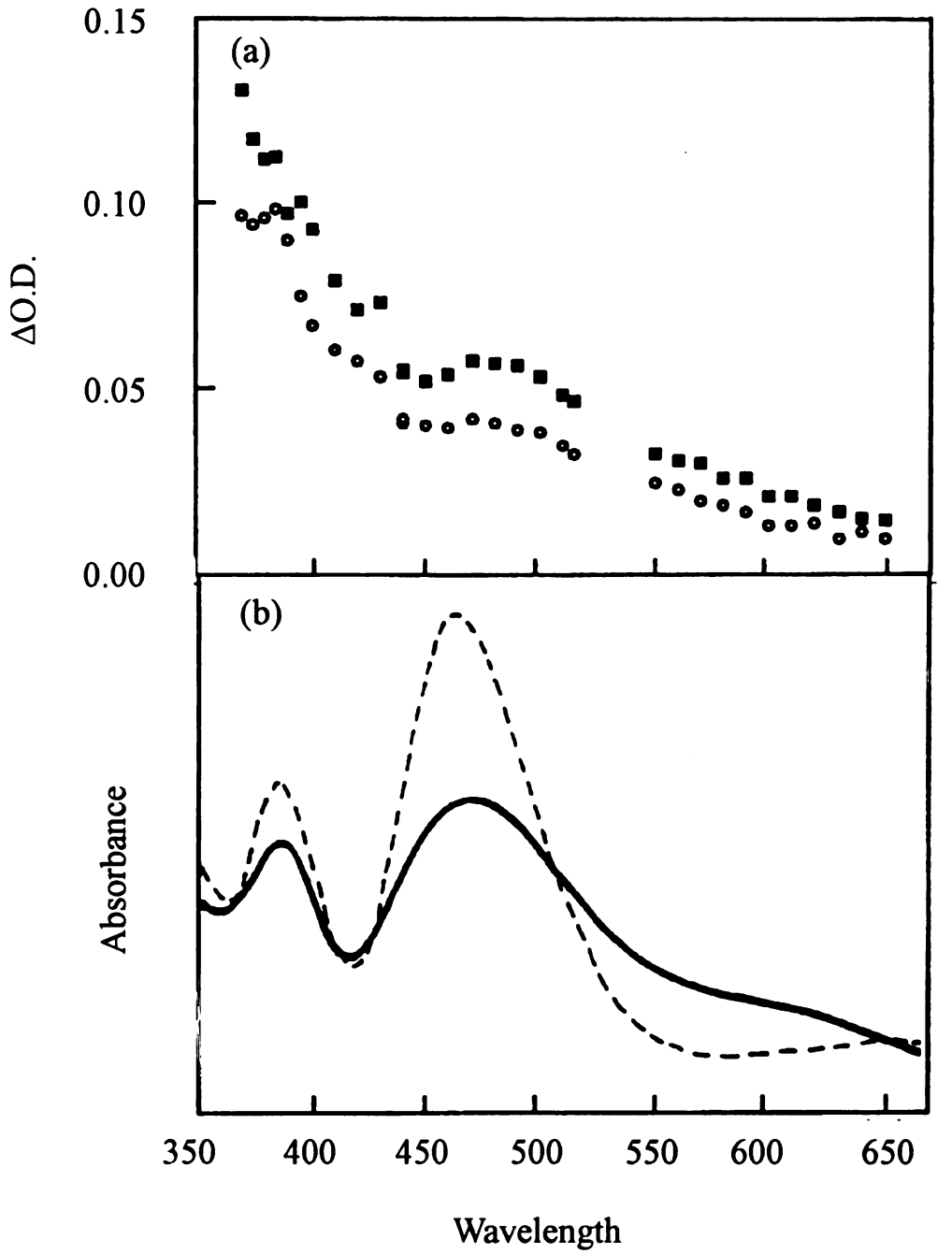

Figure I.12. (a) Transient absorption spectra of $W_2Cl_4(dppm)_2$ recorded 100 ns (solid squares) and 4 μs (open circles) after 532 nm, 10 ns excitation. (b) Absorption spectra of $W_2Cl_6(PEt_3)_4$ (-----) and $W_2Cl_6(dppm)_2$ (——) in toluene and CH_2Cl_2 repectively. Data from Reference 43.

Two-photon spectroscopy should provide access to the 2^1A_{1g} state of the δ manifold. By comparing the energy of this state with the other known energies, it will be possible to evaluate the validity of the VB model.

Chapter II

Experimental

II.A. Two-Photon Techniques

There are many ways two-photon processes can be detected. Perhaps the most obvious is two-photon absorption. This technique, however, is plagued with difficulties. Since the cross-section for a two-photon process is very small ($\delta \sim 10^{-50}$ $cm^4s^{-1}molecule^{-1}$), there is very little difference in the intensity of the emanating beam with respect to the incident beam. To avoid this problem, two-photon absorption is usually measured in very concentrated solutions using cells with long pathlengths. Also, fluctuation in laser intensity causes the signal to noise ratio to be extremely poor.

A popular technique involves the detection of ions produced by the absorption of two photons. Two common ways to perform this method are illustrated in Figure II.1. The first is for the final state to be in the ionization continuum. A second approach is to produce a final state by two-photon absorption, and before that state decomposes employ

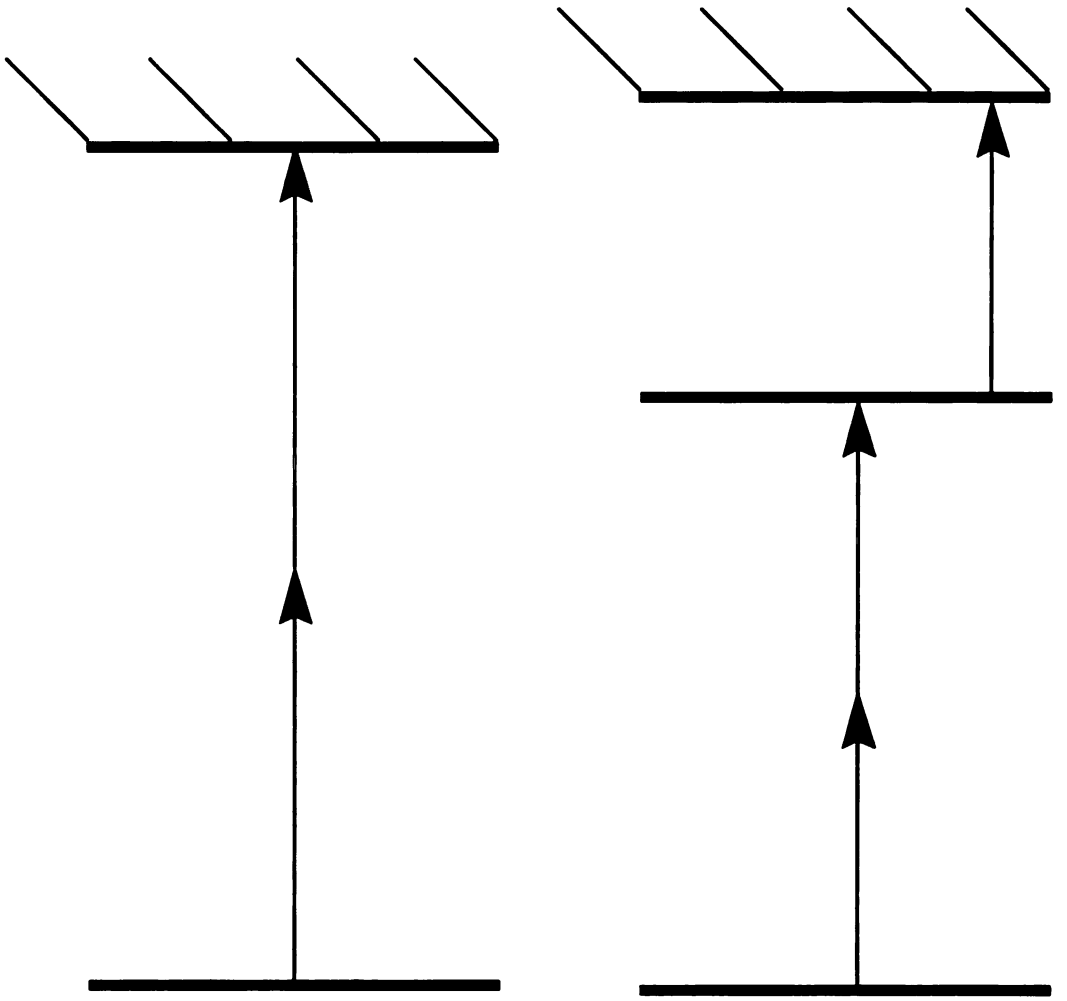

Figure II.1. Multiphoton ionization techniques. Left, two photons simultaneously absorbed through a nonresonant virtual state to the ionization continuum (2 PI). Right, two photon simultaneously absorbed to create a "final" state, which then absorbs a third photon to the ionization continuum (2+1 PI).

another laser beam to ionize to the continuum. While ionization techniques are very powerful, they are not applicable to solution phase samples.

The method most widely used to obtain solution phase spectra is two-photon excitation. In this technique, the final state decays to a lower energy, emissive state (Figure II.2). The emission is then monitored as a function of incident wavelength. Two-photon excitation is an attractive technique since it provides the low detectivity limits afforded by detecting against a dark background. Also, the emitted photons are often much higher energy than the absorbed photon. Scattered light is therefore easily discriminated against by proper filtration or use of a monochromator. Two-photon excitation is often coupled with gated integration to increase the signal-to-noise ratio even further.

II.B. Materials and Instrumentation

The compounds studied in this work, $Mo_2Cl_4(PMe_3)_4$ **(1)** and *cis*-$Mo_2Cl_2(mhp)_2(PMe_2Ph)_2$, **(2)** were prepared by Tsu-Ling Carolyn Hsu and Ann Macintosh respectively, by previously described methods[45].

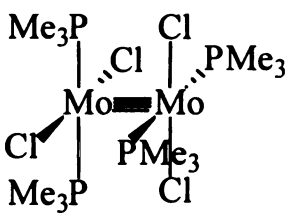

(1)

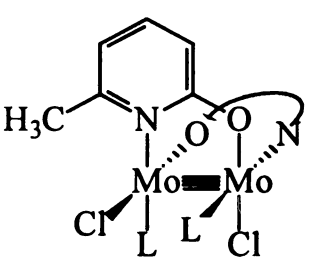

(2)

Saturated solutions were prepared in *n*-hexane (Burdick and Jackson, spectroscopic grade), which was degassed by several freeze-pump-thaw cycles. The cell used has been described previously.[46] Conventional excitation and emission spectra were acquired using a spectrometer that has been previously described also,[47] absorption spectra were measured on a Cary 2300 UV-visible spectrophotometer. The two-photon excitation

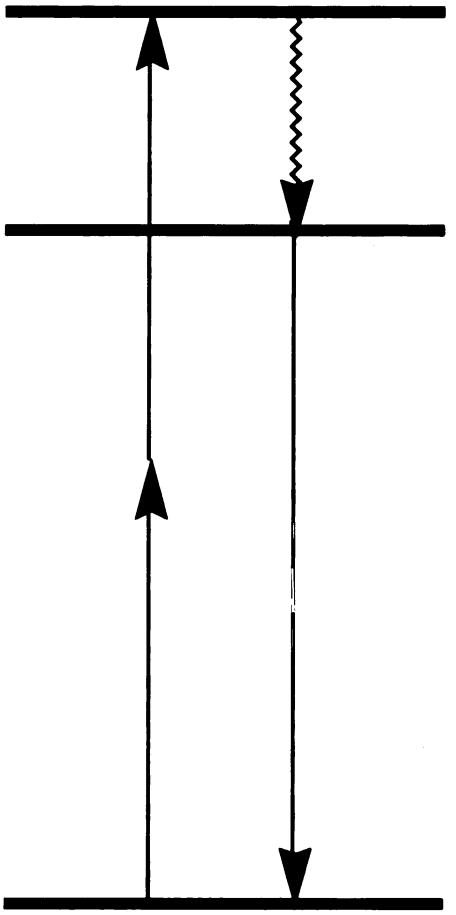

Figure II.2. Two-photon excitation spectroscopy. Two-photons are simultaneously absorbed to create an excited state, which then decays to an emissive state of lower energy.

spectra were collected in the MSU LASER Laboratory, using the instrument depicted in Figure II.3. The laser source is a Quanta-Ray DCR2-A nanosecond pulsed Nd:YAG laser whose fundamental frequency is doubled by a Quanta-Ray HGII second harmonic generator. The 532 nm output (200 mJ/pulse, 8 ns FWHM) is sent to a Quanta-Ray PDL-2 dye laser, where wavelengths from 710 nm to 970 nm can be produced using various dyes and dye combinations. The tuning curves for the dyes used are shown in Figure II.4. The laser beam is directed to the sample chamber using three prisms and a telescope. The telescope is used to maintain collimation of the laser beam and to aid in focusing the beam onto the sample.

Before reaching the sample, the laser beam is passed through three optics to provide control of the polarization of the incident radiation. The first optic is a Glan-Laser polarizer. The second and third optics are a double Fresnel rhomb and single Fresnel rhomb, respectively. These three optics, when used in series, allow for complete control of the polarization of the incident laser beam without changing the position of the laser beam. These components are described in greater detail later in this chapter. After leaving the third polarization optic, the laser beam is passed through the sample. The sample fluorescence is collected at a 90 degree angle to the incident laser beam by two f/4.0 quartz collection lenses. The fluorescence is dispersed through a monochromator and is detected by a photomultiplier tube. After the laser beam passes through the sample it is scattered through a piece of opal glass onto a photodiode, so that the relative intensity of each laser pulse can be monitored.

II.C. Two-Photon Excitation Measurement

The output signals from the photomultiplier tube and the photodiode are sent to a pair of Stanford Research Systems SR250 gated integrator/boxcar averager modules. The photodiode signal is split into two parts. The first part passes through a Phillips Scientific

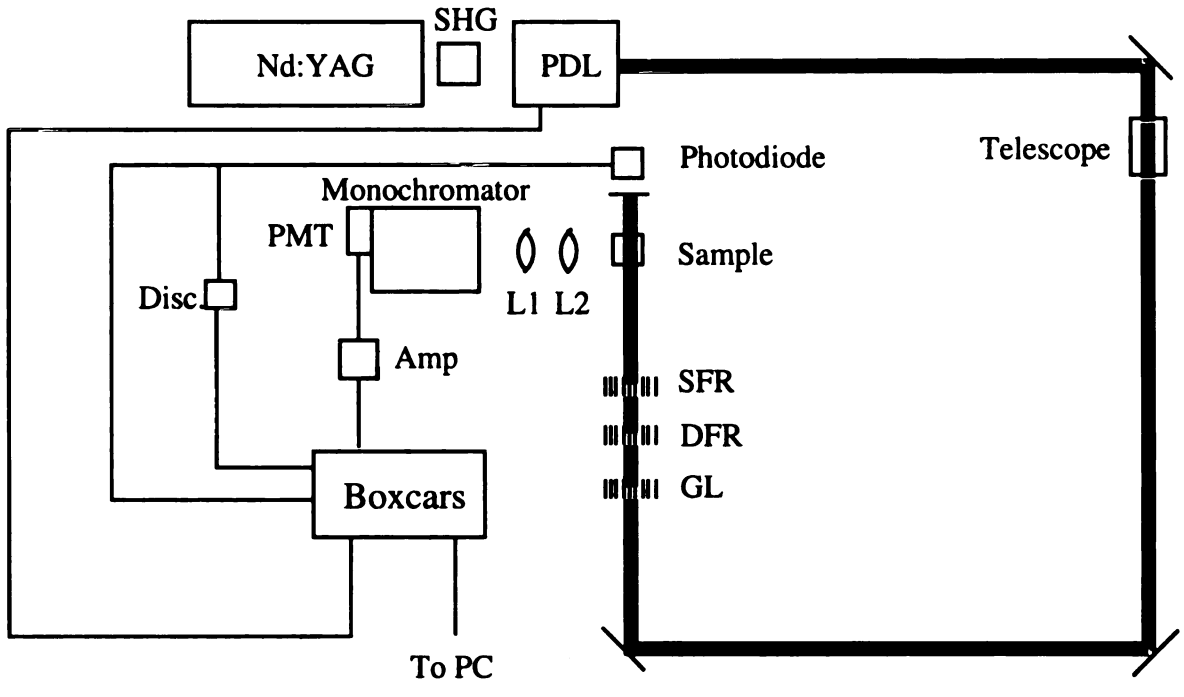

Figure II.3. Block diagram of the instrument used to collect two-photon excitation spectra. SHG second harmonic generator, PDL pulsed dye laser. GL Glan-Laser polarizer DFR double Fresnel Rhomb, SFR single Fresnel Rhomb. L1 and L2 collection lenses. PMT photomultiplier tube. Amp. Lecroy amplifier, Disc. Phillips Scientific Window discriminator, PC personal computer.

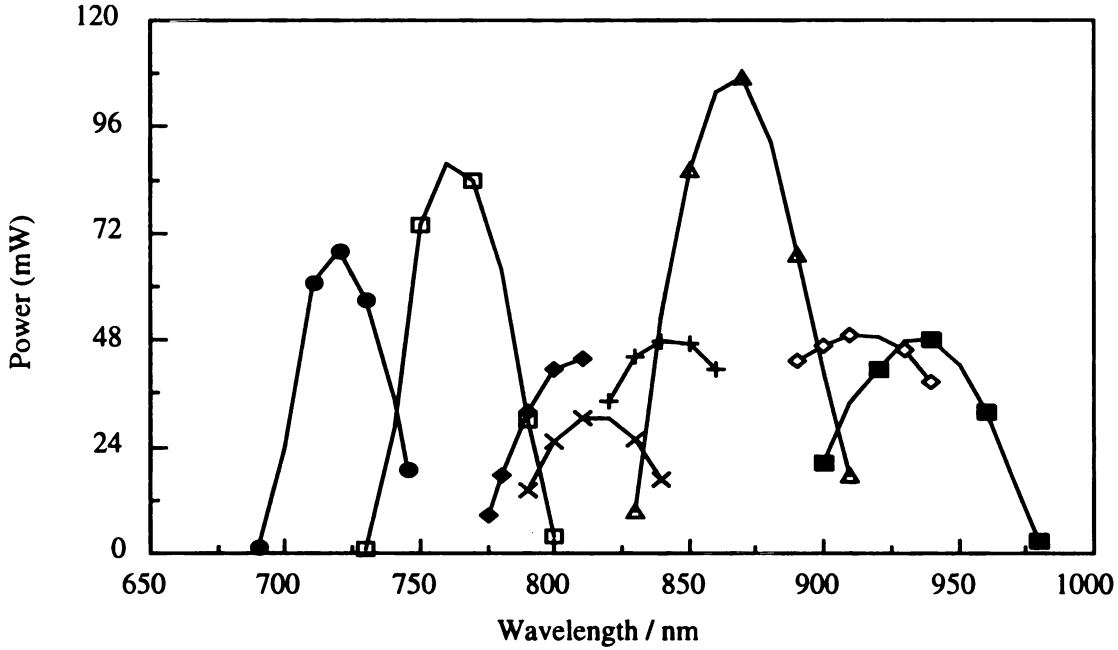

Figure II.4. Tuning curves for the laser dyes and dye combinations used: LDS 750 (solid circles), LDS 765 (open squares), LDS 765/LDS 821 (solid diamonds), LDS 821 ("x"), LDS 821/LDS 867 ("+"), LDS 867 (open triangles), LDS 867/LDS 925 (open diamonds), and LDS 925 (solid squares)

window discriminator that serves as a trigger source for the averagers. The second part goes directly to the boxcar as a measure of the laser intensity. The lower limit of the discriminator is set such that only pulses intense enough to cause the two-photon process result in a trigger of the averagers. The upper limit of the discriminator is set such that laser pulse that would saturate the photomultiplier tube do not result in trigger pulses. These limits are determined by monitoring the photodiode signal and photomultiplier signal simultaneously on an oscilloscope. Typically, 300 laser shots are averaged by the boxcars. The averaged output is sent to a personal computer where Stanford Research Systems SR267 software package is used to collect the raw photomultiplier and photodiode data for display on the monitor. After 300 shots are collected, the boxcars send an output pulse to the stepping motor of the dye laser. A device designed by Martin Rabb is used to control the step size and has been described previously.[46] For most experiments, the dye laser advanced in 0.5 nm steps. This averaging and advancing process is repeated until the desired spectral range is covered.

The raw data are sent to a program called TWOPH, which is a modification, by Dr. Jeffrey Zaleski, of the program used on the excitation spectrophotometer and has been described in great detail previously.[47] The program reads the raw photodiode and photomultiplier files and corrects for the wavelength response of the photodiode that is shown in Figure II.5. It also normalizes the photomultiplier signal by the square of the corrected photodiode signal and divides the wavelength by two to reflect the energy of the transition.

II.D. Power Dependence Measurements

The photomultiplier and photodiode signals are sent to a digital storage scope. There, the signal intensity is measured as a function of laser power. Typically 500 or 1,000 laser shots are averaged and the averaged values are placed into a spreadsheet

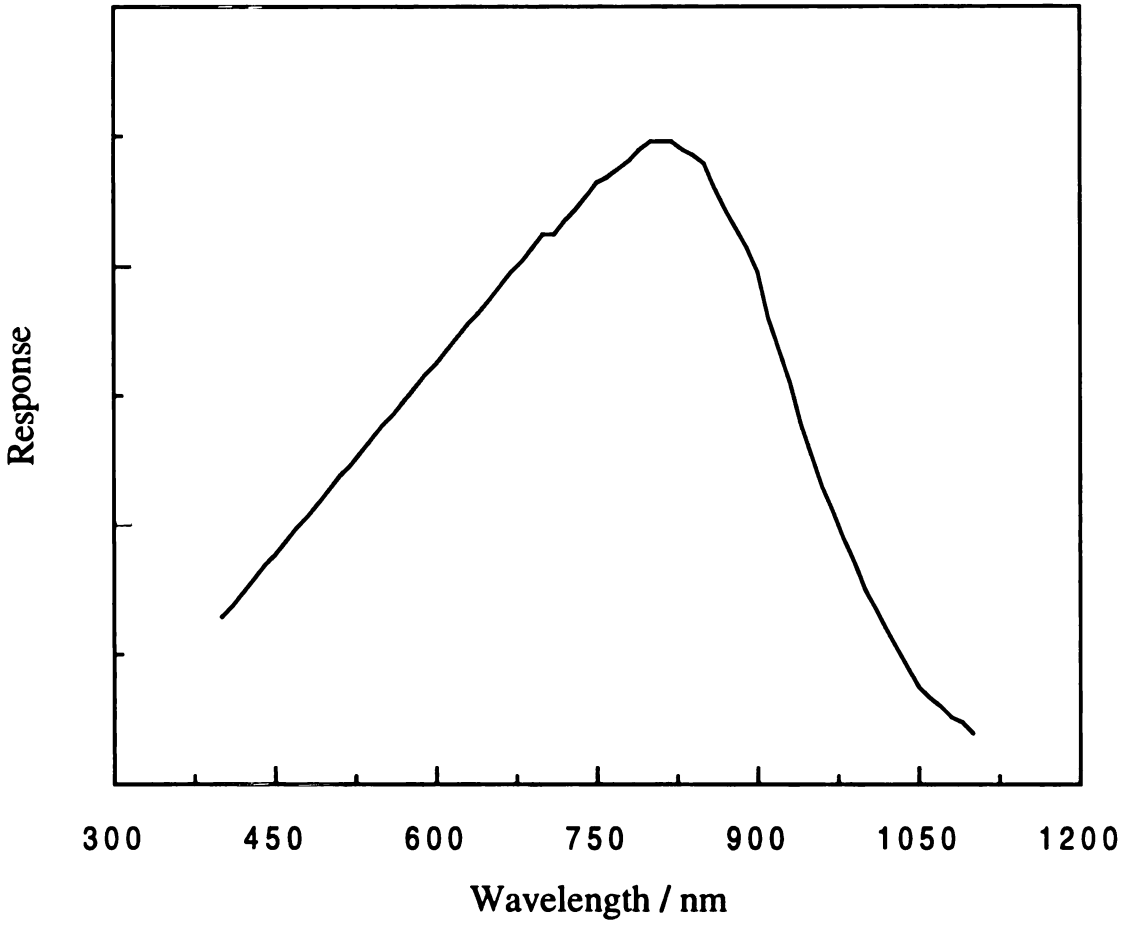

Figure II.5. Wavelength response function for the silicon photodiode used to measure the relative laser power.

program on the personal computer for manipulation. The log of the signal intensity is plotted against the log of the laser intensity and a least squares fit is performed.

II.E. Polarization Control and Polarization Ratio Measurement

The polarization of the laser beam is manipulated to be either circularly or linearly polarized by three optics. These optics are a Glan-Laser polarizer (GL), a double Fresnel rhomb (DFR) and a single Fresnel rhomb (SFR). The GL is used to maintain a constant vertical polarization of the laser beam before it reaches the next two optics. The DFR is mounted in a rotatable mount such that it can be rotated about the optical axis of the laser beam. When the DFR is rotated, the plane of polarization of the laser beam is rotated with respect to the incoming laser beam. This results in changing the plane of polarization of the laser beam with respect to the optical axis of the SFR. The SFR produces either circularly polarized or linearly polarized light depending on the plane of polarization of the incident laser beam. This is accomplished by variably retarding either the magnetic field or electric field of the laser beam. The degree of retardation is dependent upon the plane of polarization of light incident upon the SFR.

The polarization state of the laser beam is experimentally determined as shown in Figure II.6. By placing a mirror in the beam path and rotating the DFR, a minimum is observed in the reflected laser beam when the light is circularly polarized. Linearly polarized light is determined by placing a Glan-Thompson (GT) polarizer in the beam path. By rotating the DFR, a minimum is observed after the GT when the light is linearly polarized.

The polarization ratio, Ω, is determined by scanning the dye laser with the polarization optics configured such that circularly polarized light reaches the sample. The polarization optics are then reconfigured so that linearly polarized light reaches the sample and the wavelength region is scanned again. The polarization ratio is the ratio of

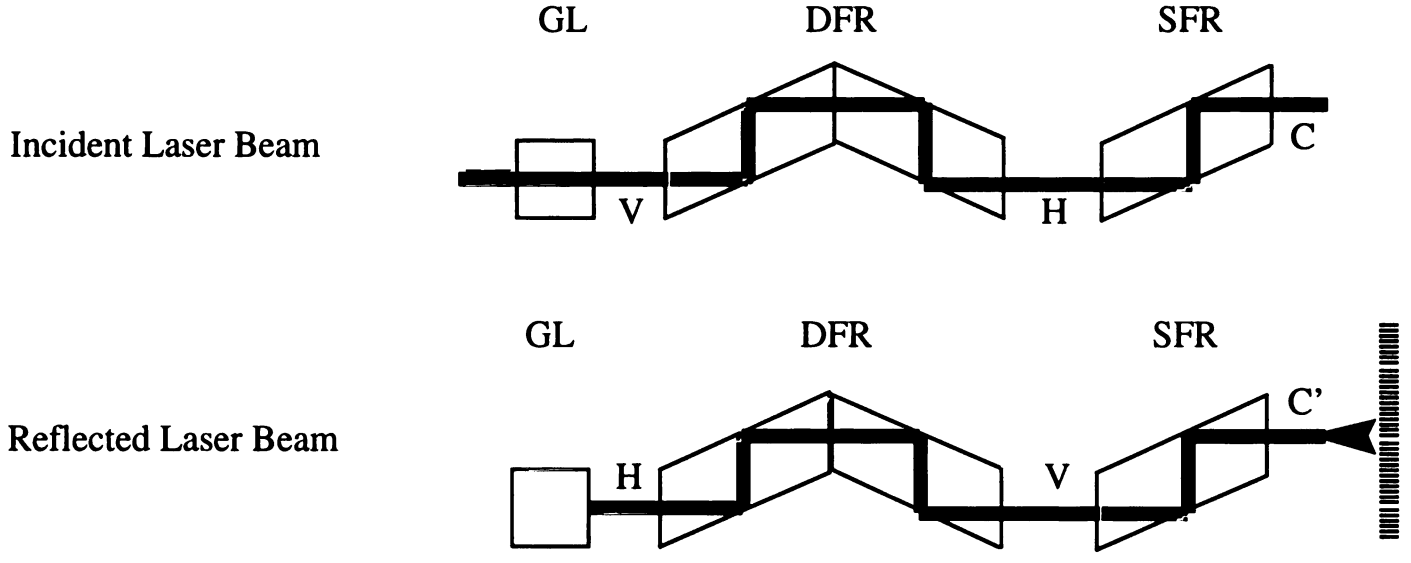

Figure II.6. Experimental determination of the polarization state. GL Glan-Laser polarizer, DFR double Fresnel Rhomb, SFR single Fresnel rhomb. H horizontal polarization, V vertical polarization, C circular polarization, C' circular polarization in the opposite sense to C

the observed signal intensity when circularly polarized light is used with respect to the intensity when linearly polarized light is used. Alternatively, the Ω measurement is made point-by-point at 5 nm increments, using the digital storage scope to measure the averaged signal intensity.

Chapter III

Results and Discussion

The valence bond model developed in the Introduction provides important qualitative descriptions of the electronic states of the δ manifold. It shows that the two low energy states ($^1A_{1g}$ and $^3A_{2u}$) can be described as diradical states, with one electron on each metal. It also suggests that the two highest energy states ($^1A_{2u}$ and 2^1A_{1g}) can be described as zwitterionic states, with two electrons on one metal, and no electrons on the other center. Also, it predicts that the energy separating the two lowest energy diradical states ($^1A_{1g}$ and $^3A_{2u}$) is equal to the energy that separates the highest energy ionic states ($^1A_{2u}$ and 2^1A_{1g}).

Several facets of this model have been experimentally confirmed. The ionic nature of the $^1\delta\delta^*$ state has been reported by Winkler and Sutin and their coworkers. They determined that the $^1\delta\delta^*$ excited state of $Mo_2Cl_4(PMe_3)_4$ possesses a dipole moment of 4.0 Debye (the ground state is apolar).[48] Also, they have shown that the $^1\delta\delta^*$ state is ionic by studying the time resolved emission spectrum.[48] The maximum of the emission spectrum shifts on the time-scale of microscopic solvent motion. This implies

that the solvent configuration around the ground state molecule (which has no dipole) does not stabilize the polar excited state and the emission spectrum evolves as the solvent reorients to stabilize the polar excited state.

The energy of the diradical triplet state ($^3A_{2u}$) has been pursued since the early 80s. As the δ bond is broken, the energy that separates the triplet state from the ground state gets smaller. There are two ways to break the δ-bond. The most obvious is to stretch the bond until the molecule dissociates. This results in the rupture of the σ and two π bonds also. A more subtle way to break the δ-bond is to twist the two halves of the molecule with respect to each other. Since the σ and two π bonds are cylindrically symmetric, they are essentially unaffected by twisting; therefore only the δ-bond is broken. As the bond is twisted to near extinction (45°), the ground state and triplet state become nearly degenerate, making it possible to populate the triplet state thermally. Gray and coworkers were the first to try to directly measure the energy of this state by measuring the temperature dependence of the paramagnetism induced by populating the triplet state of β-$Mo_2Cl_4(dmpe)_2$ [dmpe = 1,2-bis-(dimethylphosphino)ethane], which is a twisted analog (χ = 40°) of $Mo_2Cl_4(PMe_3)_4$.[49] However, the sample decomposed at moderate temperatures and a great deal of approximation and extrapolation was required to estimate the triplet state energy of the nontwisted molecule $Mo_2Cl_4(PMe_3)_4$ (5200 cm^{-1}).

Cotton *et al* have recently used a similar strategy to determine the energy of the $^3A_{2u}$ state.[50] Rather than directly observing the paramagnetism, they studied the effect of the induced paramagnetism on the NMR spectra of a series of $M_2X_4(\overset{\frown}{P\,P})_2$ complexes [$(\overset{\frown}{P\,P})$ is a bridging phosphine ligand]. By varying the $(\overset{\frown}{P\,P})$ ligand they were able to obtain a series of compounds with twist angles that spanned the range of 24.7° to 69.4° (determined from the crystal structures) which "break" the δ bond to varying extents. By studying the temperature dependence of the $^{31}P\{^1H\}$ NMR spectra of these so-called

"rotamers," it was possible to extrapolate a value for the triplet state energy of the non-twisted (or twisted 90°, depending on the definition of twist angle) $M_2X_4P_4$ molecule. They determined the energy of the $^3\delta\delta^*$ state to be 4840 cm^{-1}, which is much lower than that of the $^1\delta\delta^*$ state (17,000 cm^{-1} for $Mo_2Cl_4(PMe_3)_4$). Cotton, *et al.* also compared the triplet state energy of these molecules with the energy of their $^1\delta\delta^*$ states (Figure III.1). The energy separating these two states is essentially independent of twist angle (orbital overlap), as predicted by the VB model.[50]

The energy of the 2^1A_{1g} state, the last unobserved state in the δ manifold, has eluded spectroscopic determination because the transition from ground state is orbitally forbidden by one-photon selection rules ($g \leftrightarrow g$); the transition is also forbidden because it involves promotion of two-electrons. If this state can be observed, all of the energies of the δ manifold will be determined, thus providing a conclusive test for using the VB model to interpret the electronic states of the δ manifold.

The one- and two-photon excited emission spectra of $Mo_2Cl_4(PMe_3)_4$, (**1**), are shown in Figure III.2. The similarity of the two spectra indicates that in both cases, the emission arises from the same state, namely $^1\delta\delta^*$. This implies that the state prepared by the two-photon absorption interconverts to the $^1\delta\delta^*$ state. The corresponding spectra for *cis*-$Mo_2Cl_2(mhp)_2(PMe_2Ph)_2$, (**2**), are shown in Figure III.3. The observed emission is higher in energy than the photons absorbed in the two-photon excitation. This indicates that the excitation results from the mixing of the electric fields of two photons. The dependence of the emission intensity on the power of the incident radiation for each molecule is shown in Figure III.4 (**1**) and Figure III.5 (**2**). The log-log plots of signal intensity versus laser power have slopes of 2, which further indicates that the excitation represents a non-saturated, two-photon absorption.

The linearly polarized two-photon fluorescence excitation spectrum of $Mo_2Cl_4(PMe_3)_4$ is shown in Figure III.6, along with the one-photon fluorescence

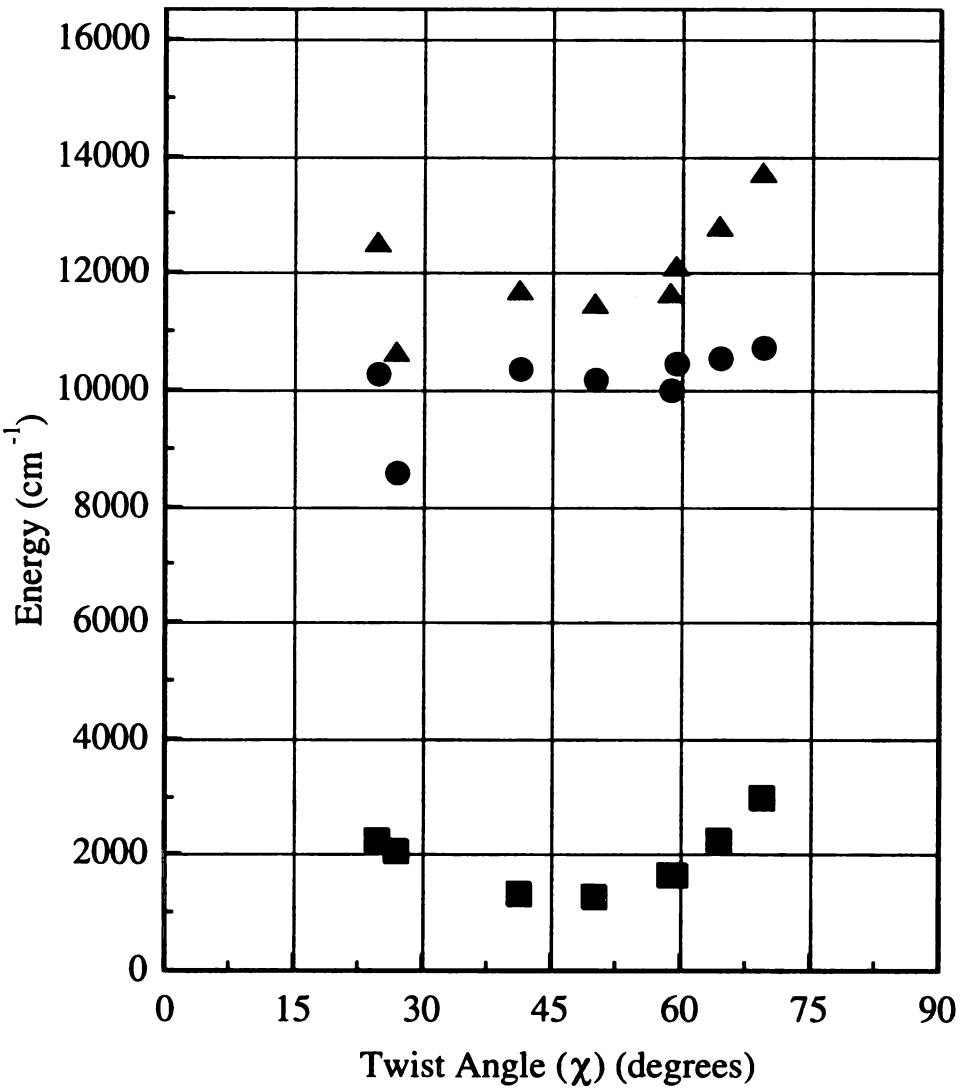

Figure III.1. Energies of $^3A_{2u}$ (solid squares), $^1A_{2u}$ (solid triangles) and the difference of the two energies (solid circles). Data from Reference 50

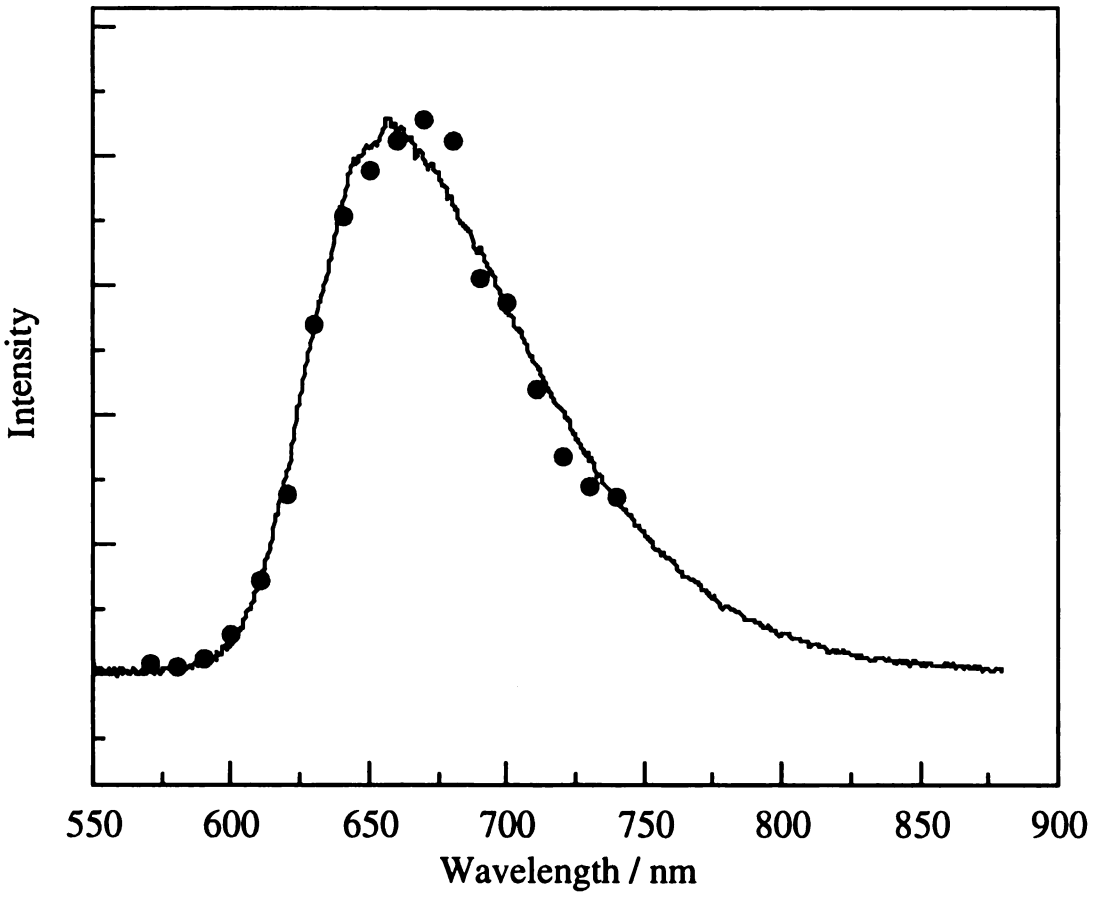

Figure III.2. One- (——) (λ_{exc}= 546 nm) and Two-photon (solid circles) (λ_{exc}= 860 nm) excited emission spectra of $Mo_2Cl_4(PMe_3)_4$

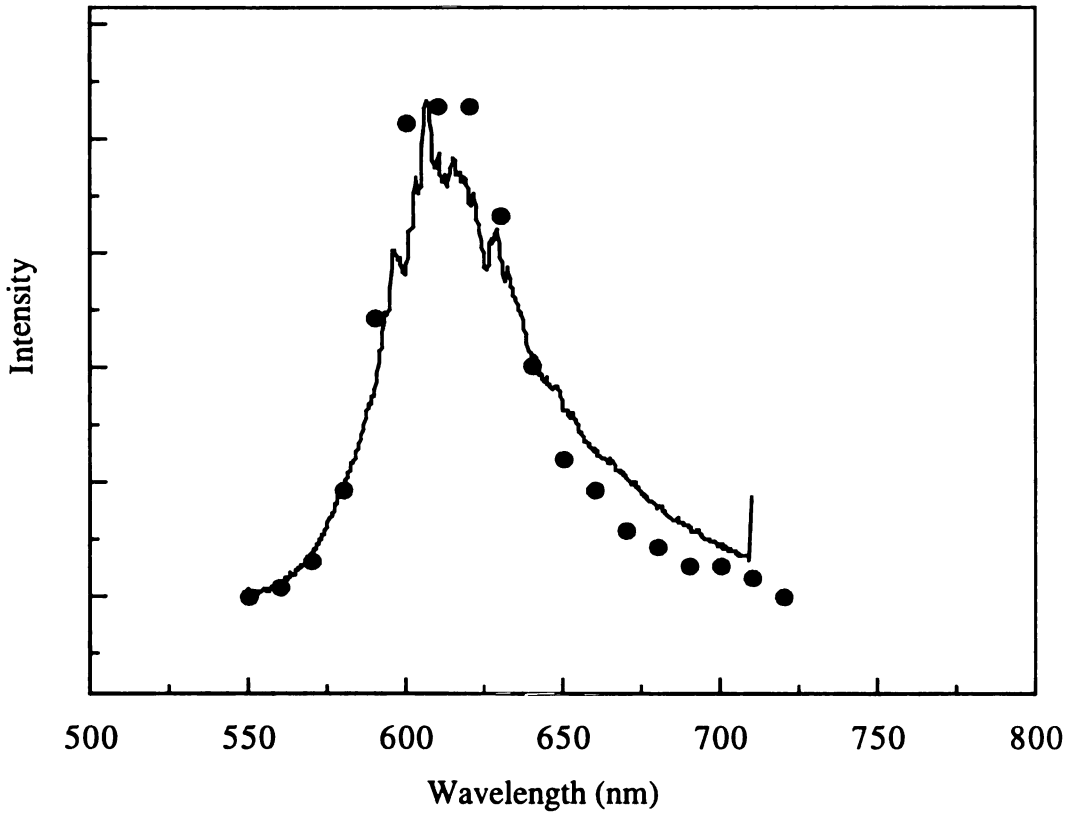

Figure III.3. One- (——) (λ_{exc}= 546 nm) and Two-photon (solid circles) (λ_{exc}= 860 nm) excited emission spectra of *cis*-$Mo_2Cl_2(mhp)_2(PMe_2Ph)_2$.

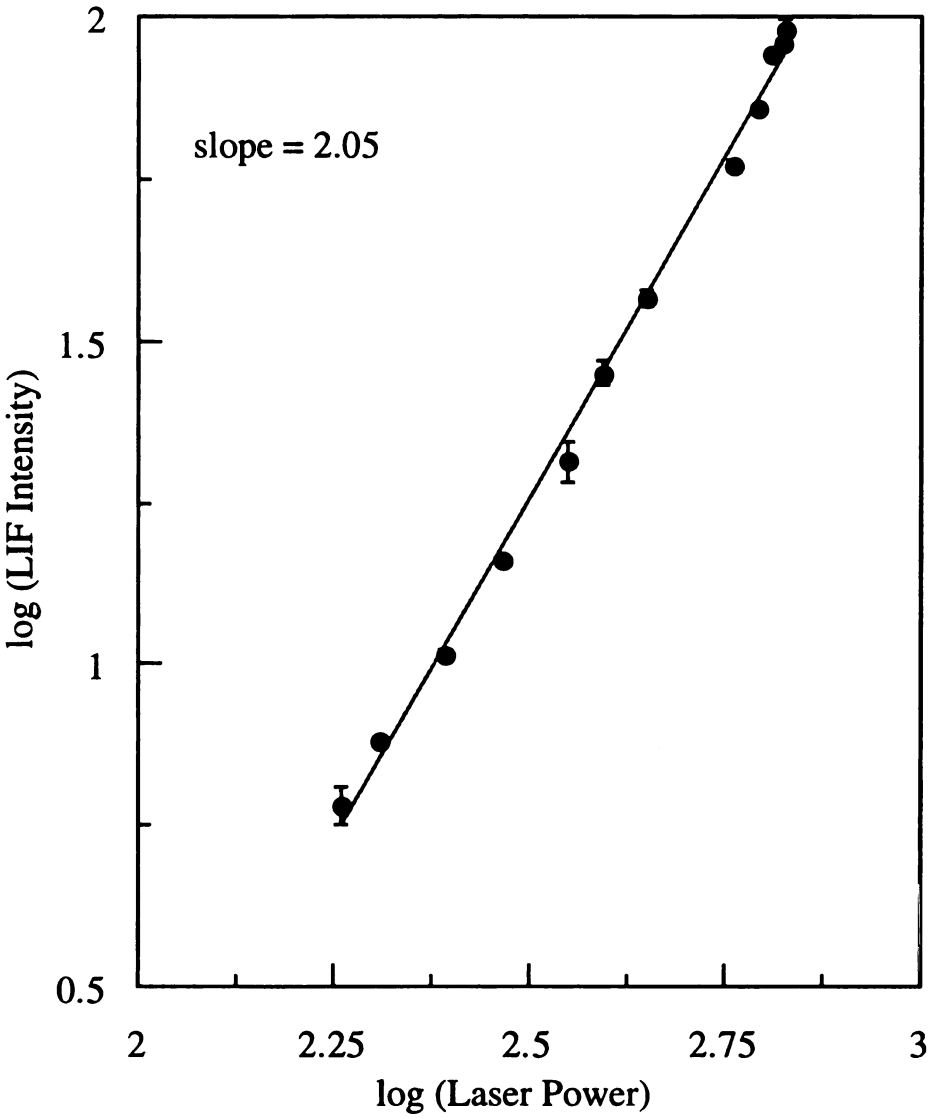

Figure III.4. Power Dependence plot for $Mo_2Cl_4(PMe_3)_4$. The instrument was configured for vertically polarized light and λ_{exc} = 860 nm. Power depencences were taken at 10 nm intervals using both polarizations, across the spectral range scanned and similar results were obtained for each.

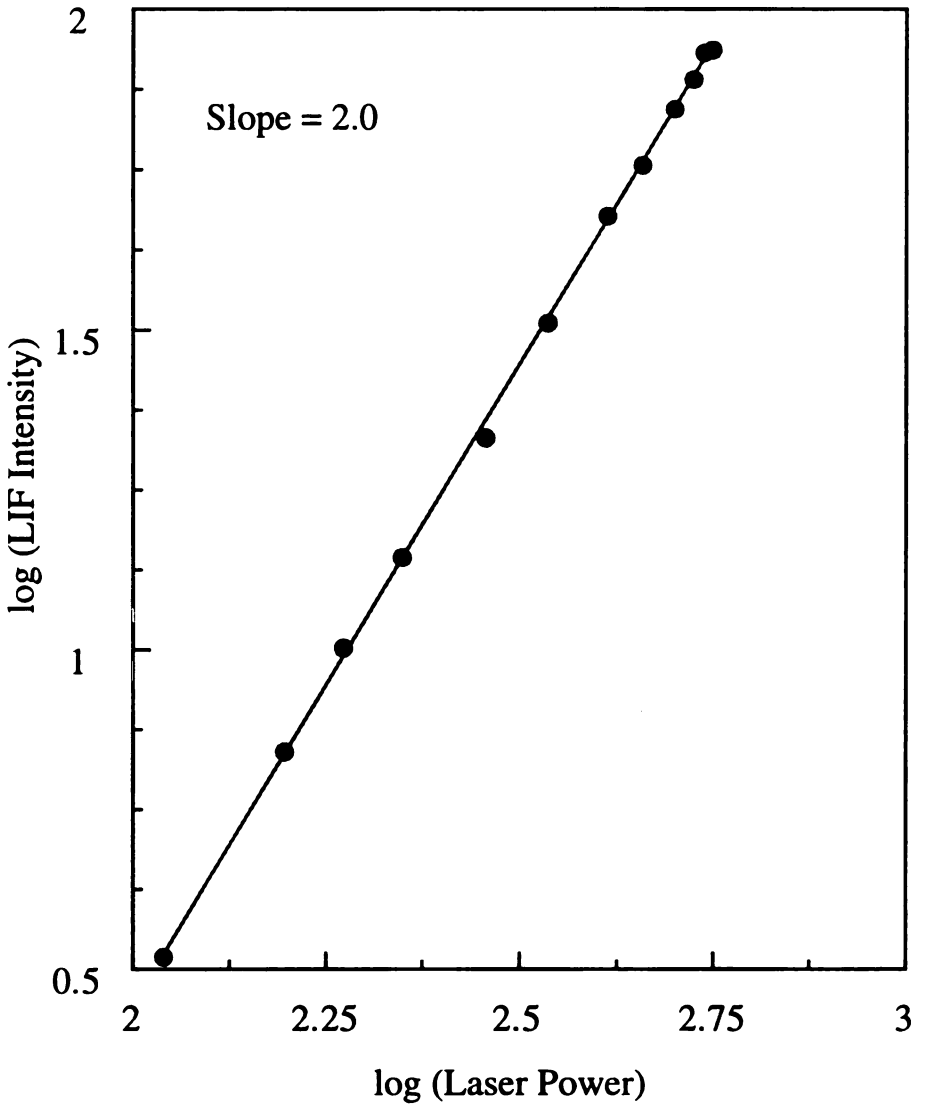

Figure III.5. Power Dependence plot for *cis*-$Mo_2Cl_2(mhp)_2(PMe_2Ph)_2$. The instrument was configured for vertically polarized light and λ_{exc} = 840 nm. Power depencences were taken at 10 nm intervals using both polarizations, across the spectral range scanned and similar results were obtained for each.

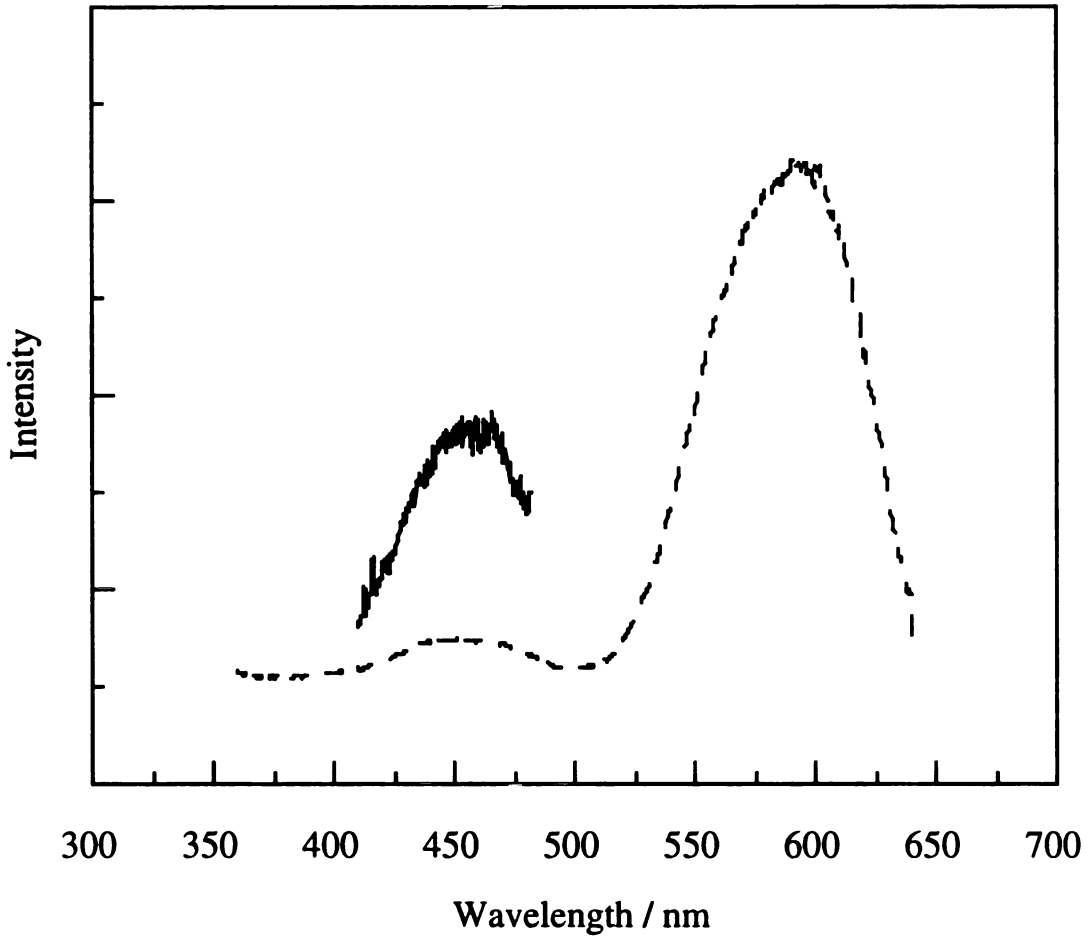

Figure III.6. One- (-----) and Two-photon (——) fluorescence excitation spectrum of $Mo_2Cl_4(PMe_3)_4$ in 3-methylpentane.

excitation spectrum. The two absorption maxima in the one-photon spectrum are assigned as indicated in Chapter I; the maximum at 445 nm is $^1(\pi\text{-}\delta^*)$ and the maximum at 585 nm is $^1(\delta\text{-}\delta^*)$. There is a single maximum observed in the two-photon spectrum, at 455 nm. To aid in assignment of the two-photon transition, it is necessary to consider all reasonable electronic transitions (those that might be expected to occur around 455 nm). As mentioned in the introduction, Hay has made extensive calculations on the $Re_2Cl_8^{2-}$ anion and determined the energies of many of the electronic transitions (both single and double excitations)[5]. While the numerical values of the transition energies will not be the same ($Re_2Cl_8^{2-}$ and the molybdenum compound of interest here, $Mo_2Cl_4(PMe_3)_4$), the relative energies can still be used to eliminate those transitions with unreasonably high or low energy. Several of the calculated transitions and their respective energies are shown in Table III.1.

The polarization ratio, Ω, is particularly useful in determining the symmetry of the states involved in a two-photon transition. Ω is plotted as a function of laser excitation wavelength in Figure III.7. The polarization ratio is constant and less than 1 across the observed band. This indicates that the observed excitation envelope represents a single electronic state and is not a convolution of several bands (unless all of the transitions have the same symmetry). Furthermore, in the D_{2d} point group, the polarization ratio can be less than one only if the symmetry of the excited state is the *same* as the symmetry of the ground state (see Table I.2 and Table I.3 in the introduction). Since it has been well established that the ground state symmetry of $Mo_2Cl_4(PMe_3)_4$ is A_1, the excited state must also be of A_1 symmetry.

There are only four reasonable (those excitations that involve either the σ or σ^* orbitals are presumed to be much higher in energy than the transition observed at 455 nm) electronic transitions that meet the requirement of an A_1 ground state and an A_1 excited state. These transitions are listed in Table III.2. By comparing these transitions

Table III.1. Selected singlet state energies for the $Re_2Cl_8^{2-}$ anion. From Reference 5.

Transition (state)	Energy with S-O* (eV)	Energy without S-O* (eV)
Single Excitations		
$\delta \rightarrow \delta^*$ ($^1A_{2u}$)	1.8	1.8
$\pi \rightarrow \delta^*$ (^1E_g)	2.6	2.5
$\delta \rightarrow \pi^*$ (^1E_g)	3.4	3.4
$\pi \rightarrow \pi^*$ ($^1A_{1u}$)	4.4	4.1
$\pi \rightarrow \pi^*$ ($^1B_{2u}$)	4.9	4.5
Double Excitations		
$\delta\delta \rightarrow \delta^*\delta^*$ ($^1A_{1g}$)	2.2	2.0
$\pi\delta \rightarrow \delta^*\delta^*$ (^1E_u)	3.6	3.4
$\delta\delta \rightarrow \delta^*\pi^*$ (^1E_u)	4.8	4.4

* S-O indicates spin-orbit coupling

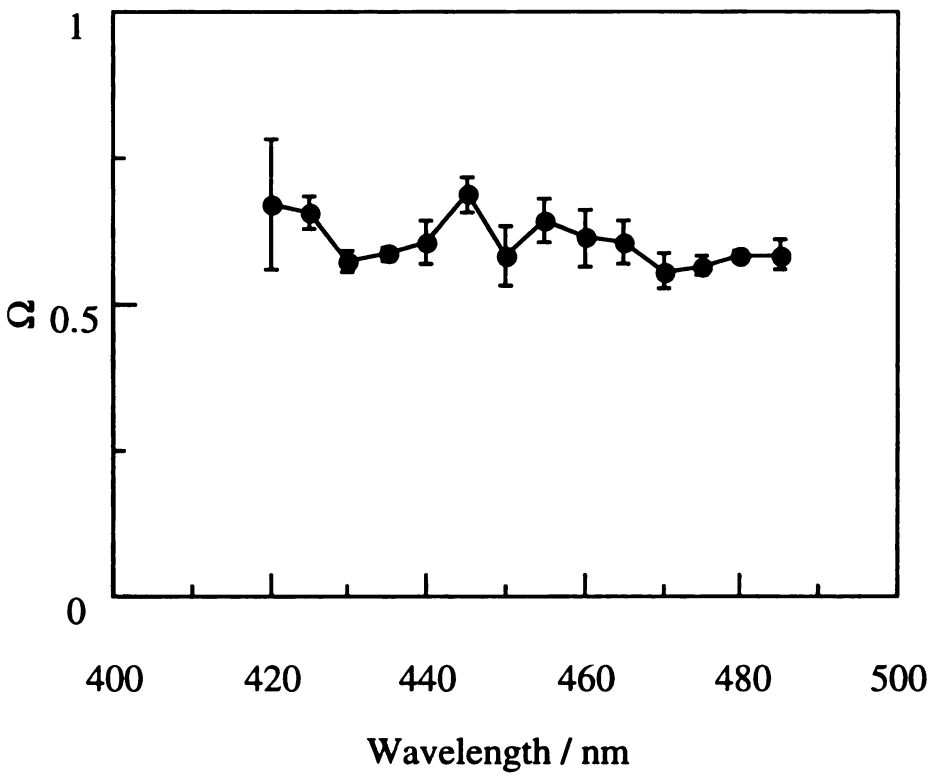

Figure III.7. Polarization ratio , Ω, for $Mo_2Cl_4(PMe_3)_4$.

Table III.2. There are twelve metal-based transitions which satisfy the criteria of an A_1 excited state and an A_1 ground state. The four transitions listed are expected to occur in the near UV or visible region of the spectrum. The remaining eight transitions involve either the σ or σ^* orbitals and should not occur in the near UV or visible region of the spectrum.

Ground State Configuration	Excited State Configuration	Transition Symmetry
$\sigma^2\pi^4\delta^2\ {}^1A_1$	$\sigma^2\pi^4\delta^0\delta^{*2}\ {}^1A_1$	$\delta\delta - \delta^*\delta^*\ (A_1 - A_1)$
$\sigma^2\pi^4\delta^2\ {}^1A_1$	$\sigma^2\pi^4\delta^0\pi^{*2}\ {}^1A_1$	$\delta\delta - \pi^*\pi^*\ (A_1 - A_1)$
$\sigma^2\pi^4\delta^2\ {}^1A_1$	$\sigma^2\pi^2\delta^2\delta^{*2}\ {}^1A_1$	$\pi\pi - \delta^*\delta^*\ (A_1 - A_1)$
$\sigma^2\pi^4\delta^2\ {}^1A_1$	$\sigma^2\pi^2\delta^2\pi^{*2}\ {}^1A_1$	$\delta\delta - \pi^*\pi^*\ (A_1 - A_1)$

with the energies determined by Hay, and the energies of the one-electron transitions for $Mo_2Cl_4(PMe_3)_4$ it can be shown that the only possibility is $\delta^2 \rightarrow \delta^{*2}$, i.e., the hitherto unseen transition in the δ manifold. Assuming that two-electron transitions are higher in energy than their one-electron counterparts allows dismissal of all the transitions but $\delta^2 \rightarrow \delta^{*2}$ (since the one-electron transitions $\pi \rightarrow \pi^*$, $\pi \rightarrow \delta^*$, and $\delta \rightarrow \pi^*$ all occur to higher energy than the observed $\delta^2 \rightarrow \delta^{*2}$ transition). This assumption is further supported by Hay's calculations that indicate that the $\delta^2 \rightarrow \delta^{*2}$ transition occur between $\pi \rightarrow \delta^*$ and $\delta \rightarrow \delta^*$ and indicate that the $\delta \rightarrow \pi^*$ and $\pi \rightarrow \pi^*$ transition occur at much higher energy than either of these two transitions. Also, Hay has calculated the energy of the $\pi\delta \rightarrow \delta^{*2}$ transition and it also lies to higher energy than the $\delta^2 \rightarrow \delta^{*2}$ transition. The $\pi\delta \rightarrow \delta^{*2}$ transition would provide a lower limit to the energy for the $\pi^2 \rightarrow \delta^{*2}$ transition. Similarly, Hay has calculated the energy of the $\delta^2 \rightarrow \delta^*\pi^*$ transition; this transition would provide a lower limit for the $\delta^2 \rightarrow \pi^{*2}$ transition energy. Assuming that the observed transition is $\delta^2 \rightarrow \delta^{*2}$ it is possible to determine the energy separating the two zwitterionic states ($^1\delta\delta^*$ and δ^{*2}). If one assumes similar Franck-Condon factors for the $^1(\delta \rightarrow \delta^*)$ transition and the $\delta^2 \rightarrow \delta^{*2}$ transition, an energy separation of 4800 cm^{-1} is calculated.

That the two-photon maximum falls so close to the $^1(\pi\text{-}\delta^*)$ transition observed in the one-photon spectrum is of some concern. As shown in Table III.3, the $^1(\pi \rightarrow \delta^*)$ transition is an allowed two-photon transition. However, the transition would be of the A_1-E type and its polarization ratio would be expected to be 1.5, rather than the observed value of 0.7. Moreover, for the transition to be allowed, two linearly polarized photons with perpendicular planes of polarization would be required (since the basis function for the E operator in the D_{2d} point group is xy), whereas the polarization of the two photons in this experiment are necessarily parallel.

Table III.3. Four possible two-photon transitions, their symmetry and the expected polarization ratio, Ω.

Transition	Symmetry	Ω
$^1(\delta^2 \rightarrow \delta^{*2})$	$A_1 - A_1$	< 1
$^1(\pi \rightarrow \delta^*)$	$A_1 - E$	3/2
$^1(\delta \rightarrow \delta^*)$	$A_1 - B_2$	3/2
$^1(\delta \rightarrow \pi^*)$	$A_1 - E$	3/2

The two-photon excitation spectrum of *cis*-$Mo_2Cl_2(mhp)_2(PMe_2Ph)_2$, shown in Figure III.8, is consistent with these assignments. There are two peaks present (λ = 390 nm and 420 nm) in this excitation spectrum. The lower energy band has a polarization ratio of ~0.7 as shown in Figure 3.10, while the polarization ratio of the higher energy band is ~1. The lower energy transition is assigned as $\delta^2 \rightarrow \delta^{*2}$, while the higher energy band is assumed to be ligand based. This is reasonable since *cis*-$Mo_2Cl_2(mhp)_2(PMe_2Ph)_2$ has such low symmetry (C_2), that a great deal of intensity borrowing may occur, thus making the ligand based transitions two-photon allowed. The energy separating $^1\delta\delta^*$ and δ^{*2} in this compound is ~5,000 cm^{-1}.

The experimentally observed triplet state energies and $^1\delta\delta^*$ and δ^{*2} energies are collected in Table III.4. By analyzing these values, it can be seen that the VB model is indeed an appropriate representation of the energies of the states of the δ manifold. The VB model predicts that the energy separating the zwitterionic $^1\delta\delta^*$ and δ^{*2} states should be equal to the triplet state energy. This is observed: δ^{*2} - $^1\delta\delta^*$ = 4800 to 5000 cm^{-1}; $^3\delta\delta^*$ = 4840 cm^{-1}. Also, the experiments performed by Cotton and coworkers showed that the energy separating $^3\delta\delta^*$ and $^1\delta\delta^*$ is essentially independent of twist angle, as predicted by the VB model.

Table III.4. Comparison of the $2^1A_{1g} - {}^1A_{2u}$ energy gap as determined by two-photon spectroscopy with the $^3A_{2u} - {}^1A_{1g}$ energy gap as measured by Cotton in Reference 50.

Compound	$^3A_{2u} - {}^1A_{1g}$ (cm^{-1})	$2^1A_{1g} - {}^1A_{2u}$ (cm^{-1})
$Mo_2Cl_4(PMe_3)_4$	4840	4800
$Mo_2Cl_2(mhp)_2(PMe_2Ph)_2$		5000

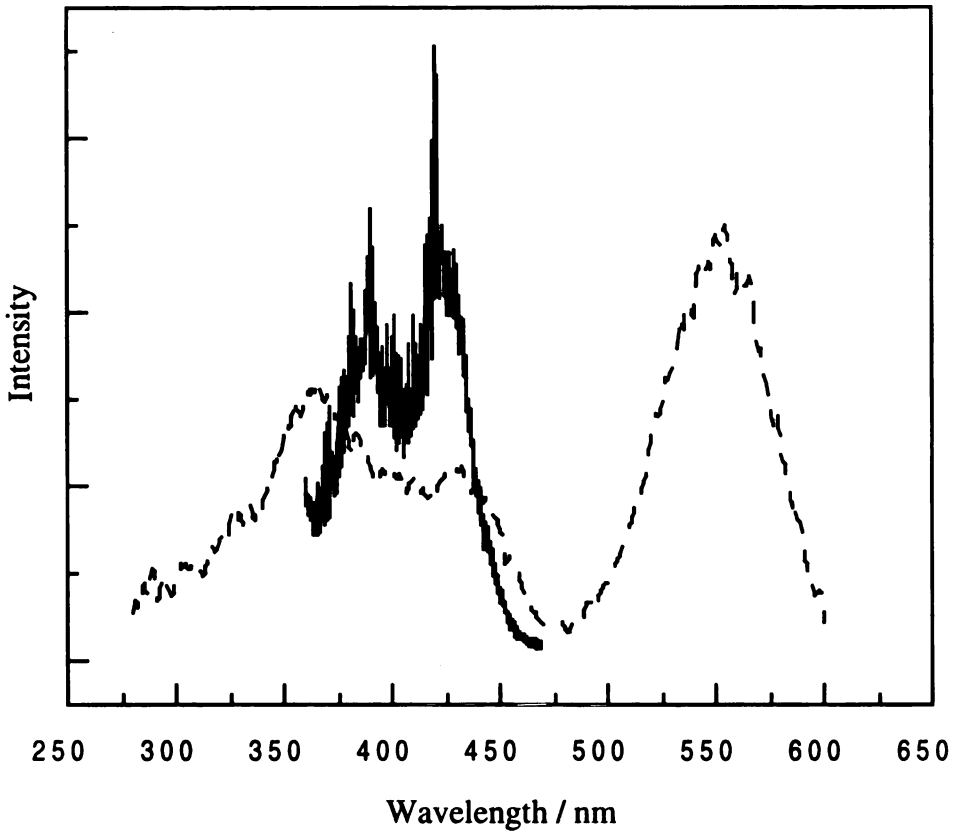

Figure III.8. One- (-----) and two-photon (——) fluorescence excitation spectrum of cis-$Mo_2Cl_2(mhp)_2(PMe_2Ph)_2$ in benzene.

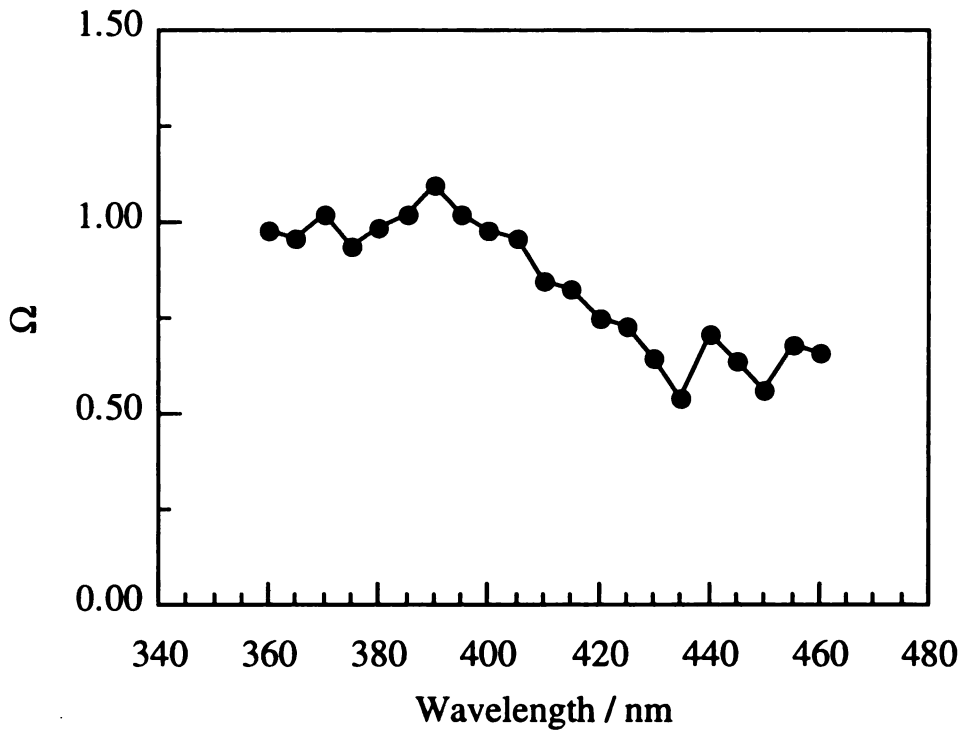

Figure III.9. Polarization ratio, Ω, for *cis*-$Mo_2Cl_2(mhp)_2(PMe_2Ph)_4$.

Appendix I

Using the states as defined in Chapter I:

$$\delta^2=\delta_1(1)\delta_1(2)\{\alpha_1\beta_2-\beta_1\alpha_2\}:{}^1A_{1g} \quad \text{(AI.a)}$$

$${}^3\delta\delta^* =\{\delta_1(1)\delta_2(2)-\delta_2(1)\delta_1(2)\}\{\alpha_1\beta_2+\beta_1\alpha_2\}:{}^3A_{2u} \quad \text{(AI.b)}$$

$${}^1\delta\delta^* =\{\delta_1(1)\delta_2(2)+\delta_2(1)\delta_1(2)\}\{\alpha_1\beta_2-\beta_1\alpha_2\}:{}^1A_{2u} \quad \text{(AI.c)}$$

$$\delta^{*2}=\delta_2(1)\delta_2(2)\{\alpha_1\beta_2-\beta_1\alpha_2\}:2^1A_{1g} \quad \text{(AI.d)}$$

And employing the Hamiltonian, also described in Chapter I:

$$\mathbf{H}_T=\mathbf{H}^{(1)}+\mathbf{H}^{(2)}+\frac{1}{\mathbf{r}_{12}} \quad \text{(AI.2)}$$

it is possible to determine the energy of each of the states.

The energies of ${}^1A_{1g}$ and 2^1A_{1g} can be determined by developing the matrix elements of the Hamiltonian. The diagonal elements represent the energy of the states and the off-diagonal elements determine the extent of mixing between the states (configuration interaction) The matrix elements for the Hamiltonian operator are:

$$H_T=\begin{pmatrix} H_{11} & H_{12} \\ H_{21} & H_{22} \end{pmatrix} \quad \text{(AI.3)}$$

The elements on the diagonal are.

$$H_{11}=\left\langle \delta^2 \left| \mathbf{H}_T \right| \delta^2 \right\rangle \quad \text{(AI.4a)}$$

$$H_{22}=\left\langle \delta^{*2} \left| \mathbf{H}_T \right| \delta^{*2} \right\rangle \quad \text{(AI.4b)}$$

The off-diagonal elements are given by:

$$H_{12}=\left\langle \delta^2 \left| \mathbf{H}_T \right| \delta^{*2} \right\rangle = H_{21}=\left\langle \delta^{*2} \left| \mathbf{H}_T \right| \delta^2 \right\rangle \quad \text{(AI.5)}$$

The energies of these Hamiltonians are:

$$H_{11} = \left\langle \delta^2 \left| \mathbf{H}^{(1)} \right| \delta^2 \right\rangle + \left\langle \delta^2 \left| \mathbf{H}^{(2)} \right| \delta^2 \right\rangle + \left\langle \delta^2 \left| \frac{1}{r_{12}} \right| \delta^2 \right\rangle \quad \text{(AI.6a)}$$

$$= \left\langle \delta_1(1)\delta_1(2) \left| \mathbf{H}^{(1)} \right| \delta_1(2)\delta_1(1) \right\rangle + \left\langle \delta_1(1)\delta_1(2) \left| \mathbf{H}^{(2)} \right| \delta_1(2)\delta_1(1) \right\rangle$$

$$+ \left\langle \delta_1(1)\delta_1(2) \left| \frac{1}{r_{12}} \right| \delta_1(2)\delta_1(1) \right\rangle \quad \text{(AI.6b)}$$

where the first term represents the energy of electron 1 in δ^2 and the second term represents the energy of electron 2 in δ^2. The third term represents the repulsive energy between the two electrons in the same orbital (δ^2). This is known as the Coulomb repulsion energy J_{11}. The energy for this state is then:

$$H_{11}=W_1(1)+W_1(2)+J_{11}(1,2)=2W_1+J_{11} \quad \text{(AI.7)}$$

where $W_1(1)$ is assumed equal to $W_1(2)$ and the electron labels have been left off.

Similarly for H_{22}, the energy of this element is:

$$H_{22}=W_2(1)+W_2(2)+J_{22}(1,2)=2W_2+J_{22} \quad \text{(AI.8)}$$

where W_2 represents the one-electron energy of an electron in the δ^* orbital and J_{22} represents the Coulomb repulsion between the two electrons in the δ^* orbital.

The energy of the off-diagonal terms is given by:

$$H_{12} = \left\langle \delta^2 \left| \mathbf{H}^{(1)} \right| \delta^{*2} \right\rangle + \left\langle \delta^2 \left| \mathbf{H}^{(2)} \right| \delta^{*2} \right\rangle + \left\langle \delta^2 \left| \frac{1}{r_{12}} \right| \delta^{*2} \right\rangle \quad \text{(AI.9a)}$$

$$= \left\langle \delta_1(1)\delta_1(2) \left| \mathbf{H}^{(1)} \right| \delta_2(1)\delta_2(2) \right\rangle + \left\langle \delta_1(1)\delta_1(2) \left| \mathbf{H}^{(2)} \right| \delta_2(1)\delta_2(2) \right\rangle$$

$$+ \left\langle \delta_1(1)\delta_1(2) \left| \frac{1}{r_{12}} \right| \delta_2(1)\delta_2(2) \right\rangle \quad \text{(AI.9b)}$$

The first two terms are zero (since $\langle \delta_1(1)\delta_1(2) \,|\, \delta_2(1)\delta_2(2) \rangle = 0$). The remaining term is the exchange energy ,K_{12}. This energy represents the energy required to move electron 1 and 2 from δ_1 to δ_2 (and *vice versa*).Therefore, the energy of the off-diagonal elements are:

$$H_{12}=H_{21}=K_{12} \quad \text{(AI.10)}$$

Including the off-diagonal elements in the secular determinant allows the energies of the states to be determined:

$$E_{^1A_{1g},2^1A_{1g}}:\begin{vmatrix}2W_1+J_{11}-\lambda & K_{12}\\ K_{12} & 2W_2+J_{22}-\lambda\end{vmatrix}=0 \qquad \text{(AI.11)}$$

Using the definitions and assumptions given in Chapter I, this secular determinant reduces to:

$$E_{^1A_{1g},2^1A_{1g}}:\begin{vmatrix}-\Delta W-\lambda & K_{12}\\ K_{12} & \Delta W-\lambda\end{vmatrix}=0 \qquad \text{(AI.12)}$$

Solving the secular determinant leads to the energies of the states:

$$E_{^1A_{1g}}=-\sqrt{K_{12}^2+\Delta W^2} \qquad \text{(AI.13a)}$$

$$E_{2^1A_{1g}}=+\sqrt{K_{12}^2+\Delta W^2} \qquad \text{(AI.13b)}$$

The next two states, $^3A_{2u}$ and $^1A_{2u}$, those with one electron in each orbital can also be determined using the same types of integrals. The only new integral to be encountered is one in which there is a Coulomb repulsion between the electrons in different orbitals:

$$\left\langle \delta_1(1)\delta_2(2)\left|\frac{1}{r_{12}}\right|\delta_1(2)\delta_2(1)\right\rangle = J_{12}(1,2) \qquad \text{(AI.14)}$$

These energies of these remaining two states are then determined to be:

$$E_{^1A_{2u}}=W_1+W_2+J_{12}+K_{12} \qquad \text{(AI.15a)}$$

$$E_{^3A_{2u}}=W_1+W_2+J_{12}-K_{12} \qquad \text{(AI.15b)}$$

REFERENCES

1. (a) Cotton, F.A. *Science* **1964**, *145*, 1305; (b) Cotton, F.A., *Inorg. Chem.* **1965**, *4*, 334

2. Cowman, C.D.; Gray, H.B. *J. Am. Chem. Soc.*, **1973**, *95*, 8177

3. Bratton, W.K., Cotton, F.A., Debeau, M., Walton, R.A. *J. Coord. Chem.* **1971**, *1*, 121

4. Benard, M. *J. Am. Chem. Soc.*, **1978**, *100*, 2354

5. Hay, P.J., *J. Am. Chem. Soc.*, **1982**, *104*, 7007

6. This is a typical value, for $Re_2Cl_8^{2-}$, the distance is 2.24Å, for more specific values, see for instance Cotton, F.A.; Walton, R.A., *Multiple Bonds Between Metal Atoms*, **1993**, *Clarendon Press*, Oxford, and references therein

7. Trogler, W.C.; Gray, H.B. *Acc. Chem. Res.* **1978**, *11*, 232

8. Mulliken, R.S., *J. Chem. Phys*, **1939**, *7*, 20

9. Bino, A; Cotton, F. A., *Angew. Chem. Int. Ed. Engl.*, **1979**, *18*, 462

10. Hopkins, M.D.; Gray, H.B., *Polyhedron*, **1987**

11. See any general chemistry text such as McQuarrie, D.A.; Rock, P.A., *General Chemistry*, **1984**, *W.H. Freeman and Company*, New York

12. Mulliken R. S. *Phys. Rev.* **1936**, *50*, 1017;1028

13. Coulson, C.A.; Fischer, I. *Philos. Mag.* **1949**, *40*, 386

14. (a) Mulliken R. S. *Phys. Rev.* **1932**, *41*, 751 (b) Mulliken R. S. *Phys. Rev.* **1933**, *43*, 297

15. (a) Dauben, W. G.; Salem, L.; Turro, N. J. *Acc. Chem. Res.* **1975**, *8*, 41 (b) Salem, L. *Pure Appl. Chem.* **1973**, *33*, 317 (c) Salem, L.; Rowland, C. *Angew. Chem. Int. Ed. Engl.* **1972**, *11*, 92.

16. (a) Dauben, W. G.; Kellogg, M. S.; Seeman, J. I.; Vietmeyer N. D.; Wendschuh, P. H. *Pure Appl. Chem.* **1973**, *33*, 317 (b) Salem, L. *Acc. Chem. Res.* **1979**, *12*, 87 (c) Tezuka, T.; Kikuchi, O.; Houk, K. N.; Paddon-Row, M. N.; Santiago, C. M.; Rondan, N. G.; Williams, J. C. Jr.; Gandour, R. W. *J. Am. Chem. Soc.* **1981**, *103*, 1367 (d)

Dauben, W. G.; Ritscher, J. S. *J. Am. Chem. Soc.* **1970**, *92*, 2925 (e) Squillacote, M. E.; Semple, T. C.; *J. Am. Chem. Soc.* **1987**, *109*, 892 (f) Childs, R. F.; DiClemiente, T.; Lund-Lucas, E. F.; Richardson, T. J.; Rogerson, C. V. *Can. J. Chem.* **1983**, *61*, 856

17. Ziegler, L. D.; Hudson, B. S. *J. Chem. Soc.* **1983**, *79*, 1197

18. (a) Schilling, C. L.; Hilinski, E. F. *J. Am. Chem. Soc.* **1988**, *110*, 2296 (b) Zimmt, M. B. *Chem. Phys. Lett.* **1989**, *160*, 564 (c) Morais, J.; Ma, J. A.; Zimmt, M. B. *J. Phys. Chem.* **1991**, *95*, 3885 (d) Schuddenboom, W; Jonker, S. A.; Warman, J. M.; de Haas, M. P.; Vermeulen, M. J. W.; Jager, W. F.; de Lange, B.; Feringa, B. L.; Fessenden, R. W. *J. Am. Chem. Soc.* **1993**, *115*, 3286 (e) Warman, J. M.; Jonker, S. A.; Schuddenboom, W; de Haas, M. P.; Paddon-Row, M. N.; Verhoeven, J. W.; Zachariasse, K. A. *Pure Appl. Chem.* **1993**, *8*, 1723 (f) Tepper, R. J.; Hooper, A. J.; Waldeck, D. H.; Zimmt, M. B. *Chem. Phys. Lett.* **1992**, *191*, 411 (g) Ma, J.; Zimmt, M. B. *J. Am. Chem. Soc.* **1992**, *114*, 9723

19. See any introductory quantum mechanics text such as Atkins, P.W., *Molecular Quantum Mechanics 2nd Ed.*, **1983**, *Oxford University Press*, New York

20. Goddard, W. A.; Dunning, T. H.; Hunt, W. J.; Hay, P. J. *Acc. Chem. Res.* **1973**, *6*, 368

21. This treatment has been generalized to the δ bond by: Hopkins, M.D.; Gray, H.B., *Polyhedron*, **1987** For a general review of this technique as originally applied to π and π^* orbitals, see :Ohno, K, *Advances in Quantum Chemistry*, **1967**

22. Ohno, K, *Advances in Quantum Chemistry*, **1967**

23. Hopkins, M.D.; Schaefer, W.P.; Bronikowski, M.J.; Woodruff, W.H.; Miskowski, V. M.; Dallinger, R.F.; Gray, H.B., *J. Am. Chem. Soc.*, **1987**, *109*, 408

24. Hopkins, M.D.; Miskowski, V.M.; Gray, H.B., *J. Am. Chem. Soc.*, **1988**, *110*, 1787

25. Hopkins, M.D.; Gray, H.B., *J. Am. Chem. Soc.*, **1984**, *106*, 2468

26. Miskowski, V.M.; Gray, H.B.; Hopkins, M.D., *Inorg. Chem.*, **1993**, *31*, 2085

27. Macintosh, A.M.; Zaleski, J.M., unpublished results

28. Macintosh, A.M., unpublished results

29. Fanwick, P.E., *Inorg. Chem.*, **1985**, *24*, 258

30. Manning, M.C., Trogler, W.C., *J. Am. Chem. Soc.*, **1983**, *105*, 5311

31. See for example Skoog, D. A. *Principles of Instrumental Analysis* **1985**, *Saunders College Publishing*, New York

32. Birge, R. in *Ultrasensitive Laser Spectroscopy* Kliger, D. S. (ed.), **1983**, Academic Press, New York

33. Friedrich, D. M. *J. Chem. Ed.*, **1982**, *59*, 472

34. See for example Fowles, G.R., *Analytical Mechanics, 4^{th} Ed.*, **1986**, *Saunders College Publishing*, New York

35. This is the time average Poynting vector, see for example Giancolli, X. Y., *Physics for Scientists and Engineers*

36. Levenson, M. D., Kano, S. S., *Introduction to Nonlinear Laser Spectroscopy*, **1988**, Academic Press Inc., New York.

37. McClain, W. M., Harris, R. A. *Two-Photon Molecular Spectroscopy in Liquids and Gases* in *Excited States*, Lim, E. C. (eds.), **1977**, Academic Press, New York

38. (a) Lin, S. H.; Fujimara, Y.; Neusser, H. J.; Schlag, E. W. *Multiphoton Spectroscopy of Molecules*, **1984**, Academic Press Inc. New York; (b) McClain, W. M., Harris, R. A. *Two-Photon Molecular Spectroscopy in Liquids and Gases* in *Excited States*, Lim, E. C. (eds.), **1977**, Academic Press, New York; (c) Birge, S. S. in *Ultrasensitive Laser Spectroscopy* Kliger, D. S. (ed.), **1983**, Academic Press, New York

39. (a) Monson, P. R.; McClain, W. M. *J. Chem. Phys.*, **1970**, *53*, 29; (b) McClain, W. M. *J. Chem. Phys.*, **1971**, *55*, 2789

40. Drago, R. S. *Physical Methods for Chemists 2^{nd} Ed.* **1992**, *Saunders College Publishing*, New York

41. Nasciemento, M. A. C. *Chem. Phys.* **1983**, *74*, 51

42. Partigianoni, C. M.; Turro, C.; Shin, Y. K.; Motry, D. H.; Kadis, J.; Dulebohn, J. I.; Nocera, D. G. In *Mixed Valency Systems: Applications in Chemistry, Physics and Biology*; Prassides, K., Ed.; Kluwer: Netherlands, 1991; pp 91-106

43. Turro, C. Ph.D. Dissertation, Michigan State University, 1992

44. Similar long-lived transients are also seen for $Mo_2Cl_4(dmpm)_2$ (τ = 100 μs)

45. $Mo_2Cl_4(PMe_3)_4$: Cotton, F. A.; Extine, M. W.; Felthouse, T. R.; Kolthammer, B. W.; Lay, D. G. *J. Am. Chem. Soc.* **1981**, *103*, 4040 $Mo_2Cl_2(mhp)_2(PMe_2Ph)_2$: Fanwick, P.E., *Inorg. Chem.*, **1985**, *24*, 258

46. Yu, J. Ph. D. Dissertation, Michigan State University (1990)

47. Newsham, M. Ph. D. Dissertation, Michigan State University (1988)

48 Zhang, X., Kozik, M.; Sutin, N.; Winkler, J.R.; in Bolton, J.R.; Mataga, N.; McLendon, G. (eds.), *Electron Transfer in Inorganic, Organic, and Biological Systems*, **1991**, *Advances in Chemistry Series No. 228 (American Chemical Society)*, Washington, D.C., 247

49. Hopkins, M.D.; Zietlow, T.C.; Miskowski, V.M.; Gray, H.B., *J. Am. Chem. Soc.*, **1985**, *107*, 510

50. (a) Cotton, F.A.; Eglin, J.L.; Hong, B.; James, C.A., *J. Am. Chem. Soc.*, **1992**, *114*, 4915. (b) Cotton, F.A.; Eglin, J.L.; Hong, B.; James, C.A., *Inorg. Chem.*, **1993**, *32*, 2104.


MICHIGAN STATE UNIVERSITY LIBRARIES
3 1293 02343 3349